

A STUDY OF THE PRODUCTION AND PROPERTIES OF CHARMED  
BARYONS

BY

KRISHNA M. PODURI

The University of Mississippi

August 1994

© Copyright 1994

by

Krishna Meher Podury

**All Rights Reserved**

# Acknowledgements

I would like to thank Dr. Lucien M. Cremaldi for his invaluable guidance and assistance in the preparation and writing of this thesis. Without his patience and understanding this work would have been impossible.

I would like to thank Dr. Kumar Bhatt and Dr. Don J. Summers for their participation and input as my committee members.

I would also like to thank Dr. Krishna Swamy Gounder for his support, Dr. Ali Rafatian for his immense help in writing the thesis and Mr. Kevin Hendrix for keeping the systems intact 24hrs a day. Ms. Danying Yi and Mr. Yangzhao Sun deserve special thanks for helping me strip the data.

Finally, I would like to thank my parents for giving me this opportunity to work in United States, my sisters, brother and friends for their continual love and support which has been invaluable.

# Contents

Acknowledgements	i
List of Tables	iv
List of Figures	v
<b>1 Introduction</b>	<b>1</b>
1.1 Introduction . . . . .	1
1.2 Hadroproduction of Charm . . . . .	2
1.3 $\Lambda_c$ production . . . . .	3
1.4 Excited Charm Production . . . . .	5
1.5 Dalitz plot & $K^{\bar{0}*}$ resonance in $\Lambda_c \rightarrow pK\pi$ . . . . .	6
1.6 Double Charm . . . . .	6
<b>2 Detector &amp; Data</b>	<b>7</b>
2.1 Beam Production . . . . .	7
2.2 Target . . . . .	8
2.3 Spectrometer . . . . .	10
2.4 Particle Identification . . . . .	13
2.5 Data . . . . .	15
2.6 Farm Reconstruction . . . . .	16
<b>3 Analysis of Data</b>	<b>20</b>
3.1 Vertexing and Filtering of Events . . . . .	20

3.2	Stripping . . . . .	21
3.3	Analysis . . . . .	29
<b>4</b>	<b>Conclusions</b>	<b>40</b>
4.1	Measurements with $\Lambda_c \rightarrow pK\pi$ . . . . .	40
4.2	$\Sigma_c$ measurements . . . . .	43
4.3	$\Lambda_c \rightarrow pK^{*\bar{0}}$ measurement . . . . .	43
4.4	Summary . . . . .	44
	<b>Bibliography</b>	<b>45</b>

# List of Tables

2.1	The five-foil target layout . . . . .	9
2.2	Cherenkov Counter Particle Momentum Thresholds GeV/c. . . . .	13
3.1	Summary of cuts used at several stages of analysis . . . . .	24
3.2	Number of observed $\Lambda_c \rightarrow pK\pi$ events and fitted mass differences . .	31
3.3	$X_F$ analysis $\Lambda_c^\pm$ . . . . .	31
3.4	Number of observed $\Sigma_c$ and fitted masses(MeV/c <sup>2</sup> ). . . . .	33
4.1	Comparison of production measurements with NA32 . . . . .	42
4.2	$\Sigma_c$ production measurements. . . . .	43

# List of Figures

1.1	The QCD picture of the hadroproduction of charm through gluon fusion and $q\bar{q}$ annihilation. . . . .	2
1.2	Associated production of $\Lambda_c D^-$ . . . . .	4
2.1	The position of the primary vertex in the Z-axis. . . . .	9
2.2	E791 spectrometer . . . . .	11
2.3	The momenta and the cherenkov probabilities of p, K and $\pi$ on $\Lambda_c \rightarrow pK\pi$ substrip. . . . .	14
2.4	Cumulative number of events processed at Umiss starting November 1992 until July 1994. . . . .	17
2.5	Display of a reconstructed event. . . . .	19
3.1	Illustration of SDZ. . . . .	21
3.2	Illustration of the DIP and PTB cuts. . . . .	23
3.3	The spectra of selection parameters for the vertices and tracks from data collected on the final substrip. . . . .	25
3.4	Detector efficiency vs $X_F$ determined from Monte Carlo events. . . . .	26
3.5	Some distributions found in Monte Carlo events. . . . .	27
3.6	Some distributions found in data events. . . . .	28
3.7	The $M_{pK\pi}$ fitted mass spectrum. . . . .	30
3.8	Acceptance corrected $X_F$ spectrum fitted to $\frac{dN}{dX_F} = (1 -  X_F )^n$ . . . . .	32
3.9	$\Sigma_c$ fitted mass plots: (A) $\Sigma_c$ sum plot (B) $\Sigma_c^{++}$ plot (C) $\Sigma_c^0$ plot and $M_{\Lambda_c \rightarrow pK\pi}$ plot with SDZ > 6, PTB < 0.50 GeV/c and $\text{PROB}_{pK\pi} > 0.20$ .	34
3.10	Dalitz plot $M_{K\pi}^2$ vs $M_{p\pi}^2$ (GeV/c <sup>2</sup> ) <sup>2</sup> . . . . .	36

3.11	The $M_{K\pi}$ spectrum from all $\Lambda_c$ events, $2.26 \leq M_{pK\pi} \leq 2.32$ (GeV/ $c^2$ ).	37
3.12	$M_{pK\pi}$ with $K^{\bar{*}0}$ mass constraint. . . . .	38

# Chapter 1

## Introduction

### 1.1 Introduction

Charm is one of the six quarks, incorporated into the standard model of Weinberg and Salam [1]. Bjorken suggested [2] and Glashow [3] postulated its existence to suppress flavor changing neutral currents, the GIM mechanism. The charm quark was experimentally discovered in 1974 in the form of the  $J/\Psi(c\bar{c})$  particle at SLAC and BNL [4]. Many charmed mesons and baryons were discovered soon after. [5]

Charm is considered, by most, the first heavy quark,  $m_c \simeq 1.5\text{GeV}/c^2$ , and theorists have been able to study its production and decay through perturbation techniques. Meaningful comparisons between experiment and theory have been possible. In this thesis we will study the properties of charmed baryons, made when a charmed quark ( $c$ ) combines with two light quarks ( $u$  or  $d$  or  $s$ ). The  $\Lambda_c$  ( $cud$ ) is the lightest charmed baryon ( $M_{\Lambda_c} = 2.285\text{GeV}/c^2$ ) and the easiest to produce.

This thesis focuses on the study of  $\Lambda_c$ 's produced in experiment E791, performed at Fermi National Accelerator Laboratory in 1991. This experiment has produced the largest sample of charmed particles to date and many of our results will be statistically superior to current results in charmed baryon physics. This thesis also represents a first report on charmed baryons from E791, using 364 of the total 575 runs available, or about 2/3 of the data set.

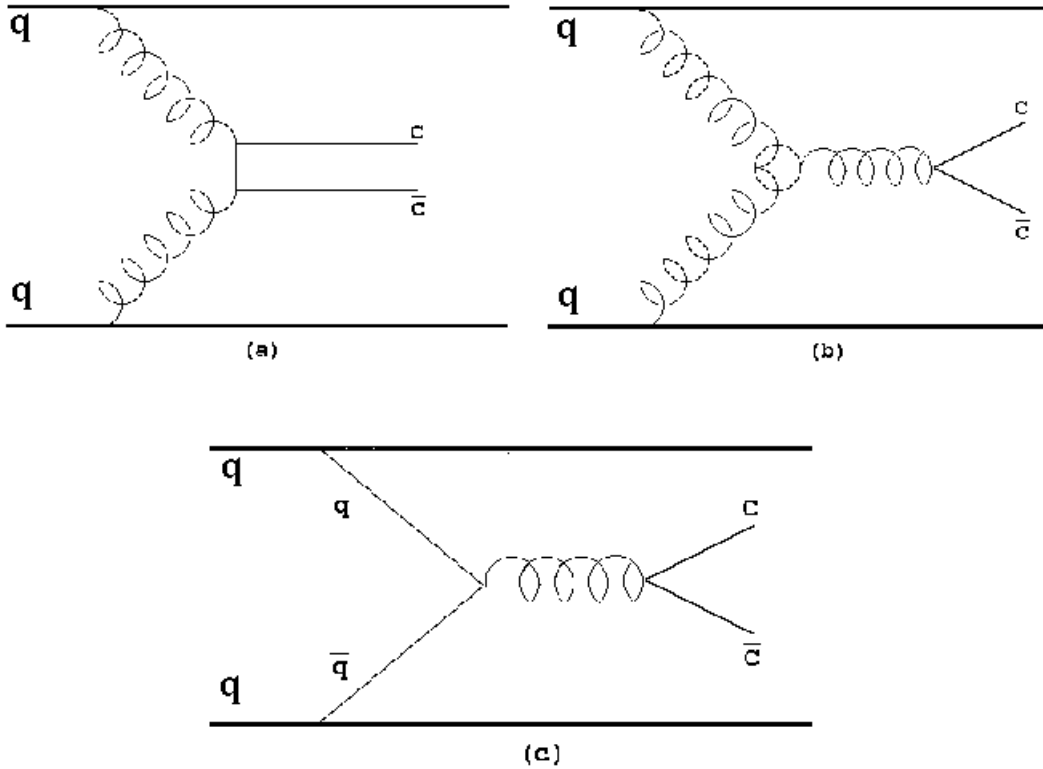


Figure 1.1: The QCD picture of the hadroproduction of charm through gluon fusion and  $q\bar{q}$  annihilation.

## 1.2 Hadroproduction of Charm

Charmed particles are produced in hadronic collisions. The hadroproduction of charm is a complex process and discussed in detail many places [6]. One can attempt to explain the charm production through QCD and the parton model. In this picture (1.1) the hadroproduction of charm is a process that involves the hard scattering of two partons  $i$  and  $j$ , one from each colliding hadron  $A$  and  $B$ . The charm production cross-section [7] is described by a convolution of the parton-parton differential cross section  $\frac{d\hat{\sigma}_{ij}}{d\hat{x}_F}$  and the parton structure function (probability density) of  $F(x, Q^2)$ . The charm pair ( $c\bar{c}$ ) differential cross section with respect to Feynman- $x$  is

$$\frac{d\sigma_{c,\bar{c}}}{d\hat{x}_F} = \sum_{i,j} \int dx_A dx_B \left[ \frac{d\hat{\sigma}_{ij}(x_A P_A, x_B P_B, \hat{p}, m_c, Q^2)}{d\hat{x}_F} \right] F_i^A(x_A, Q^2) F_j^B(x_B, Q^2) \quad (1.1)$$

Where  $\hat{p}$  and  $m_c$  are the momentum and the mass of the charmed quark.  $F_i^{A/B}(x_{A/B}, Q^2)$  gives the probability of finding parton  $i$  with momentum fraction  $x$  in hadron  $A/B$ .

$Q$  is the typical momentum transfer between the parton and the charm quark. The Feynman- $x$  variable,  $\hat{x}_F$  is defined as

$$\hat{x}_F = \frac{\hat{p}_z}{p_{\max}} \simeq \frac{2\hat{p}_z}{\sqrt{s}} \quad . \quad (1.2)$$

where  $\hat{p}_z$  is the momentum of the charm quark in the direction of the incident hadron and  $\sqrt{s}$  is the center of mass energy. The summation  $i$  and  $j$  are over the parton indices. In the Figure(1.1) the contributing subprocesses for  $c\bar{c}$  production in hadronic collisions are shown for the lowest order. Processes (a) and (b) are thought to dominate when  $\sqrt{s} \gg 2m_c$ , as in our case. Recent calculations[7] give the total cross section,  $\sigma_{c\bar{c}}$ , to be about  $15\mu\text{b}/N$ (microbarns per nucleon). This is in general agreement with latest measurements.

After the  $c\bar{c}$  quarks are created, they hadronize into charmed baryons and mesons by combining with light sea quarks or quarks from the beam or target hadrons. This fragmentation occurs with unit probability, thus the  $c\bar{c}$  cross section should closely approximate the observed charm particle production cross sections. Experimentalists observe the number of charmed particles per  $X_F = 2p_{\Lambda_c}/\sqrt{s}$  or  $dN/dX_F$ . This spectrum peaks strongly at  $X_F = 0$  and falls rapidly. It is usually parameterized as  $dN/dX_F = (1 - |X_F|)^m$ ,  $m = 3.0 - 5.0$  .

### 1.3 $\Lambda_c$ production

E791 produced charmed baryons by colliding a  $500\text{GeV}/c$   $\pi^-$  beam into a nuclear target. A schematic of the associated production process is shown in the next page

$$\pi^- + N \longrightarrow \Lambda_c D^- + X \quad . \quad (1.3)$$

In the above equation  $X$  represents additional hadrons produced in the interaction. The threshold energy for this interaction to occur is

$$E_{th} = M_{\Lambda_c} + M_{D^-} + M_X \simeq 4.5\text{GeV} \quad . \quad (1.4)$$

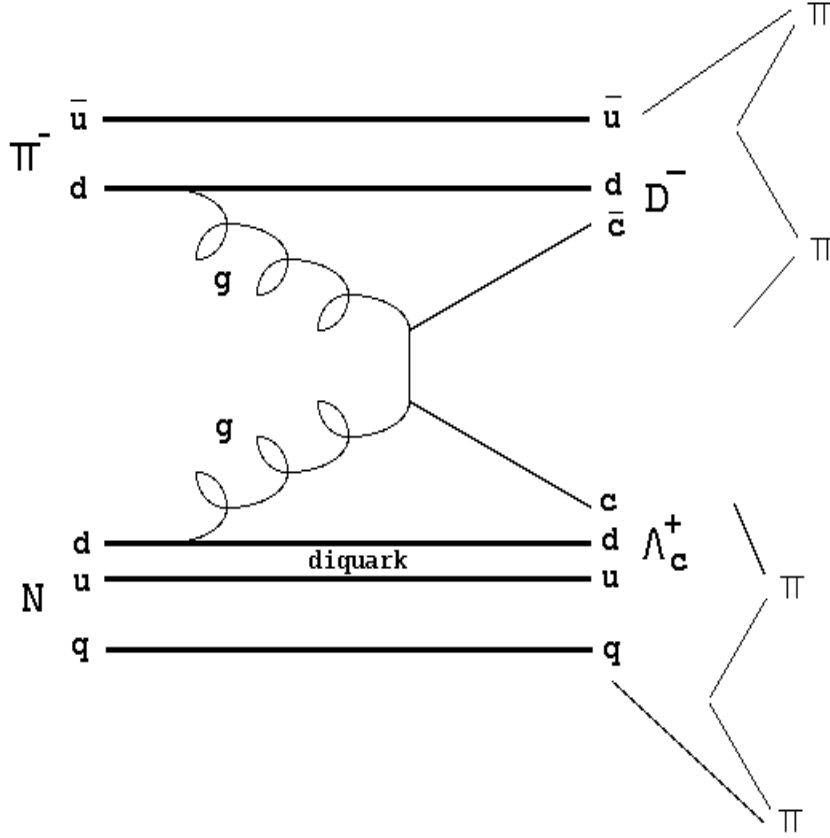


Figure 1.2: Associated production of  $\Lambda_c D^-$ .

Since the  $\pi N$  center of mass energy is  $E_{cm} \simeq \sqrt{2m_N E_\pi} = \sqrt{5000} \simeq 33 GeV$ , charmed baryon production will occur quite readily. The NA32 [8] collaboration has set the production level of  $\Lambda_c$  particles in the  $\pi N$  interactions to be approximately  $\sigma_{\pi N \rightarrow \Lambda_c X} \simeq 4 \mu b/N$ . The interaction cross-section for the pions to interact in a nuclear target is about  $23 mb/N$ . Thus, charmed baryons will be created about every  $10^{-3}$  interactions.

E791 has recorded  $20 \times 10^9$  interactions. An estimate of the number of charmed baryons ( $\Lambda_c$ ) produced in these interactions is

$$N_{\Lambda_c} \simeq N_{int} \left( \frac{2 \times \sigma_{\Lambda_c}}{\sigma_{inelastic}} \right) \times BR_{pk\pi} \times \epsilon_{trig} \times \epsilon_{recon} \quad (1.5)$$

$$N_{int} = 20 \times 10^9$$

$$\epsilon_{trig} \times \epsilon_{recon} = 0.5 \times 10^{-3}$$

$$\left( \frac{\sigma_{\Lambda_c}}{\sigma_{inelastic}} \right) = \left( \frac{4}{23} \right) \times 10^{-3}$$

$$BR_{pk\pi} = 4\%$$

$$N_{\Lambda_c} \simeq 1400$$

In the  $\Lambda_c \bar{D}^-$  associated production process shown in figure 1.2 the  $\Lambda_c$  would be

produced at low or even negative  $X_F$  since it is made from a diquark(du) in the target fragment. It would be accompanied by a fast moving  $D^-$  in the lab frame at higher  $X_F$ . Symmetric production of  $\Lambda_c^+\Lambda_c^-$  can also occur if the  $c$  and  $\bar{c}$  are dressed from the sea. We can measure the ratio of these production mechanisms by taking the ratio of  $N_{\Lambda_c^+}/N_{\Lambda_c^-}$

$$\frac{N_{\Lambda_c^+}}{N_{\Lambda_c^-}} = \frac{\sigma_{\Lambda_c^+D^-} \times \epsilon_1 + \sigma_{\Lambda_c^+\Lambda_c^-} \times \epsilon_2}{\sigma_{\Lambda_c^-D^+} \times \epsilon_1 + \sigma_{\Lambda_c^+\Lambda_c^-} \times \epsilon_2} \quad (1.6)$$

The factors  $\epsilon_1$  and  $\epsilon_2$  are the efficiency of reconstruction for the slightly different production modes. We might assume that  $\sigma_{\Lambda_c^-D^+} \times \epsilon_1$  production is negligible because it is difficult to produce an antibaryon from the sea, then,

$$\frac{N_{\Lambda_c^+}}{N_{\Lambda_c^-}} \simeq 1 + \frac{\sigma_{\Lambda_c^+D^-} \times \epsilon_1}{\sigma_{\Lambda_c^+\Lambda_c^-} \times \epsilon_2}. \quad (1.7)$$

We can then get the ratio of  $\sigma_{\Lambda_c^+D^-}/\sigma_{\Lambda_c^+\Lambda_c^-}$  after  $\epsilon_1$  and  $\epsilon_2$  are determined from Monte Carlo studies or by other means. In addition, we should also observe more  $D^-$  than  $D^+$  mesons in about the same ratio from the same argument.

## 1.4 Excited Charm Production

It is possible that in the hadroproduction of charm excited spin and isospin states may be favored. The  $c\bar{c}$  pair can hadronize into excited charmed baryon states. Such candidates are the  $\Sigma_c(2455)$  isospin triplet  $\Sigma_c^{++}, \Sigma_c^+,$  and  $\Sigma_c^0$  formed through  $\pi^-N \rightarrow \Sigma_c\bar{D}X$  or  $\pi^-N \rightarrow \Sigma_c\bar{\Lambda}_cX$ .

The  $\Sigma_c$  states decay hadronically, with lifetimes of  $10^{-23}$ s, to  $\Lambda_c\pi$  states. The pion is emitted almost instantly and the  $\Lambda_c$  will live for about 0.2ps before it decays. We can search for  $\Sigma_c^{++}$  and  $\Sigma_c^0$  through the decays  $\Sigma_c^{++} \rightarrow \Lambda_c^+\pi^+$  and  $\Sigma_c^0 \rightarrow \Lambda_c^+\pi^-$ . These decays have never before been clearly seen in hadronic interactions. We expect the ratio of  $\sigma_{\Sigma_c}/\sigma_{\Lambda_c} \simeq 10\%$  from measurements in  $e^+e^-$  collisions and photoproduction.[9]

We can express the ratio of observed  $\Sigma_c$  to  $\Lambda_c$  events as

$$\frac{N_{\Sigma_c}^{obs}}{N_{\Lambda_c}^{obs}} = \frac{N_{\Sigma_c}}{N_{\Lambda_c}} \times \frac{BR(\Sigma_c \rightarrow \Lambda_c\pi).BR(\Lambda_c \rightarrow pK\pi)}{BR(\Lambda_c \rightarrow pK\pi)} \times \frac{\epsilon_{pK\pi\pi}}{\epsilon_{pK\pi}} \quad (1.8)$$

After some reduction we obtain the true ratios of  $\Sigma_c$ 's to  $\Lambda_c$ 's produced as

$$\frac{N_{\Sigma_c}}{N_{\Lambda_c}} = \frac{N_{\Sigma_c}^{obs}}{N_{\Lambda_c}^{obs}} \times \frac{\epsilon_{pK\pi}}{\epsilon_{pK\pi\pi}} \quad (1.9)$$

$\epsilon_{pK\pi\pi}$  and  $\epsilon_{pK\pi}$  are the efficiencies for the reconstructing the 4 and 3 body states respectively in the spectrometer and  $BR(\Sigma_c \rightarrow \Lambda_c\pi) = 1$ .

## 1.5 Dalitz plot & $K^{\bar{0}*}$ resonance in $\Lambda_c \rightarrow pK\pi$

The  $\Lambda_c$  will decay about 4% of the time into a  $pK\pi$  final state. There is a strong tendency for the formation of a  $K^{\bar{0}*}$  and thus  $\Lambda_c \rightarrow pK^{\bar{0}*}$  and then  $K^{\bar{0}*} \rightarrow K^-\pi^+$ . The best measurement on the branching ratio of  $\Lambda_c \rightarrow pK^{\bar{0}*}$  is given as

$$\frac{BR(\Lambda_c \rightarrow p\bar{K}^{*0})}{BR(\Lambda_c \rightarrow pk\pi)} = 0.36 \pm 0.10[5] \quad (1.10)$$

With as many as 1400  $\Lambda_c \rightarrow pK\pi$  decays we can reduce the error on this measurement considerably.

A Dalitz plot analysis [10] can be used to search for resonance and spin structure in the matrix element of the  $\Lambda_c \rightarrow pK\pi$  decay. The relativistic three-body decay rate can be written as

$$d\Gamma_{pK\pi} = 1/(2\pi)^2 \times M_{pK\pi} \times \mathbf{M}^2 dm_{K\pi}^2 dm_{p\pi}^2 \quad (1.11)$$

$\mathbf{M}$  is the matrix element. If  $\mathbf{M}$  is constant we should see a uniformly populated Dalitz plot. If resonances are present, they appear as Breit-Wigner shaped enhancements. Only two of the three two-body masses are independent and thus a plot of  $m_{K\pi}^2$  vs  $m_{p\pi}^2$  will show all resonance structures.

## 1.6 Double Charm

Events in which both charm particles  $\Lambda_c\bar{D}$  or  $\Lambda_c^+\Lambda_c^-$  are observed can tell us the most about the production process. Even with a sample of 1000-2000 inclusive decays we expect only a few decays in which the second charmed particle is also seen. We will search for such decays and possibly obtain a limit on our sensitivity, if none are seen.

# Chapter 2

## Detector & Data

The E791 fixed target experiment was conducted at the Fermi National Laboratory from July 1991 to January 1992. E791 used an upgraded Tagged Photon Spectrometer first commissioned by E516 in 1979 and subsequently used for many charm experiments including E791. In the following chapters I'll give a short description of the experiment. Further details can be found elsewhere. [11]

### 2.1 Beam Production

The Fermilab accelerator produces a 800GeV primary proton beam. It is produced in a multistep process. Firstly, negative hydrogen ions are produced by passing neutral hydrogen over a cesium source. The ions are accelerated to an energy of 750KeV and injected into the Linear Accelerator (LINAC). In the second stage the LINAC accelerates this negative hydrogen beam to 200MeV and bunches them into buckets with 19ns spacing. The ions are then stripped of both the electrons and the resulting proton beam is passed into the third stage. During the 3rd stage the 8GeV booster ring injects the buckets into the 150GeV Main ring. In the 4th stage, the main ring accelerates the protons and these are injected into the Tevatron that accelerates the beam to an energy of 800GeV. This entire process takes about 34 secs and results in approximately  $2 \times 10^{13}$  protons orbiting in the Tevatron in a 56 second cycle. In the

remaining 22 seconds of each minute the proton beam is extracted from the accelerator and directed to the target experiments. Then the cycle repeats itself.

This extracted primary proton beam is then bombarded on an upstream beryllium target of 30cm thickness which generates numerous pions. These negative pions are momentum filtered and collimated to produce the 500GeV/c beam used in the experiment. Quadrupole and dipole magnets transport and focus this beam into a narrow parallel stream of negative pions, before striking the experiment's targets.

## 2.2 Target

The E791 target[12] consist of five foils (1 Platinum and 4 Carbon) arranged coaxially in a plexiglass holder, fixing the foils at a precise separation. The platinum foil was selected for its high  $Z$  and high density. This helps in having a thinner foil yet attaining high interaction length. The platinum foil is made from a polished Australian mint coin. The platinum foil is 0.5mm thick and the other four carbon (Diamond) foils are 1.5mm thick. The five targets represent about 2% of a pion interaction length. The primary vertex position in  $z$  is shown in the figure 2.1. The primary vertices are essentially formed due to the interaction in the targets. Table 2.1 shows the five foil target layout.

The target separation is chosen such that a charmed particle produced in one foil typically decayed before the next foil downstream. The mean decay length is less than 1cm and the foils are spaced roughly 1.5cm apart. The mean decay length  $l$  can be calculated using

$$l = \beta\gamma c\tau = \frac{p}{m}\tau$$

where  $p$  and  $m$  are the measured momentum and mass of the  $\Lambda_c$ .

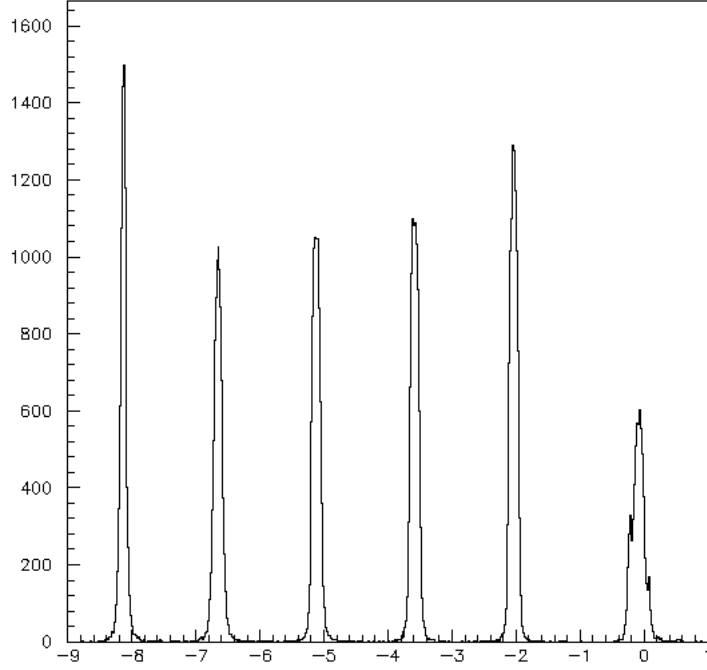


Figure 2.1: The position of the primary vertex in the Z-axis.

foil number	1	2	3	4	5
$z$ -position (cm)	-8.191	-6.690	-5.154	-3.594	-2.060
material	Pt	C	C	C	C
spacing(cm)		1.501	1.536	1.560	1.534
thickness (mm)	0.52	1.57	1.57	1.53	1.58
interaction length	0.588 %	0.412 %	0.412 %	0.402 %	0.415 %

Table 2.1: The five-foil target layout

## 2.3 Spectrometer

The Tagged Photon Spectrometer (TPS) is a large-acceptance two-magnet spectrometer equipped with silicon-microstrip detectors (SMD's), drift chambers, two Cherenkov counters and electromagnetic, hadronic calorimetry and the muon detector. This spectrometer has been extensively described elsewhere[11]. The schematic of the E791 detector is shown in the figure 2.2.

### Silicon Microstrip Detector

The Silicon Microstrip Detectors (SMD's) are very essential for particle tracking near the target region and resolving the decay vertices. They provide accurate vertex information due to their fine segmentation. To increase the tracking and reconstruction efficiency, six new planes down stream were added for E791 bringing the number of downstream planes to 17. These planes were oriented in X, Y and V planes, where V planes were rotated 20.5 degrees with respect to the vertical X-axis.

Each SMD plane consists of a 300 micron thick sandwich of aluminium strips, arsenic and boron doped silicon, and an aluminium base that creates a reverse p-i-n type diode.

When a charged particle passes through the SMD plane it deposits its ionization energy. This creates electron-hole pairs in the semiconductor which are separated by applying a bias voltage. Narrow aluminium strips deposited on top of the semiconducting silicon wafer provide a conducting path for the freed charge particles. By connecting electrodes to the individual strip a small electrical pulse can be collected and amplified, giving the location of the incident particle. A series of silicon plates with strips with a pitch of a few tens of microns provides an accurate tracking device suitable for resolving separated vertices due to charm decays.

### Proportional Wire Chambers

Two downstream Proportional wire Chambers (PWCs) were used to increase the track resolution and for tracking redundancy. A gas mixture of 82.7% Argon, 17%

TAGGED PHOTON SPECTROMETER  
E791

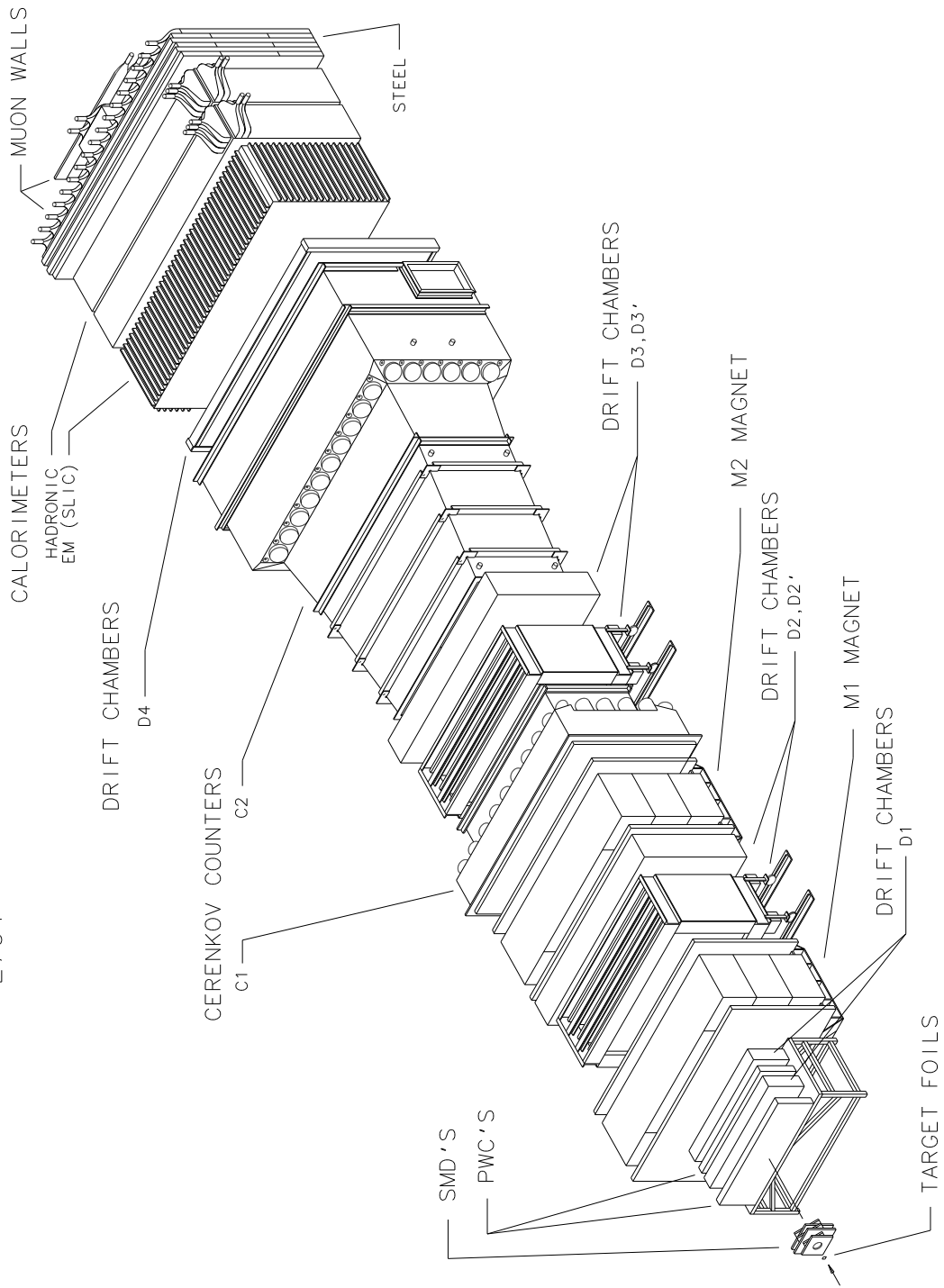


Figure 2.2: E791 spectrometer

CO<sub>2</sub> and 0.3% Freon was used. The spacing between the wires is 2mm producing a resolution of about 600microns ( $2\text{mm}/\sqrt{12} = 577\mu\text{m}$ ).

### **Drift Chambers**

The Tagged Photon Spectrometer was equipped with four modules of planar drift chambers. A total of 35 planes measuring four different views, X, X', U and V were distributed through seven separate gas boxes. The X and X' views were made of vertically strung wires with the X' view shifted by half a cell relative to the X planes.

The 1st chamber (module) D1 was located upstream of the 1st analysis magnet M1 and along with the SMD's and PWC's, provided an initial measurement of the track trajectory. D2 was positioned between the two bend magnets. D3 was located just after the 2nd bend magnet M2 and added tracking information for particles with momentum high enough to make it through both the magnets. The last chamber D4 was positioned much downstream after the cherenkov counters and just before the calorimeters.

A drift chamber plane consists of three planes of wires, two planes of high voltage(HV) cathode wires and one plane of sense wires and field shaping wires. The sense wires were 25micron gold plated tungsten while the HV wires were 125micron Be-Cu. The HV plates were typically held at about -2.4kV while the field shaping wires were at about -2.0kV. The sense wires were grounded. Adjacent planes of sense wires in the same assembly shared the same high voltage plane between them.

When a charged particle passed through a drift chamber it ionized the gas in the chamber. For E791 the gas used was a mixture of 89% Argon, 10% Carbon dioxide and 1% CF<sub>4</sub>. The electrons produced are then amplified and collected by the sense wires due to the field produced by the negative HV and field planes. The signal collected is then amplified further and passed through a discriminator, allowing adjustments to the signal to noise ratio.

### **Magnets**

The Tagged Photon Spectrometer had two magnets which are placed in between

Particle Type	C1 Momentum Threshold (GeV/c)	C2 Momentum Threshold (GeV/c).
$\pi$	5.35	10.5
$K$	18.7	37.2
$p$	35.5	70.7
$e$	0.0193	0.0385
$\mu$	4.01	7.99

Table 2.2: Cherenkov Counter Particle Momentum Thresholds GeV/c.

the D1 and D2, and D2 and the 1st Cherenkov counter respectively. These magnets provided transverse momentum kicks of 212MeV/c and 320MeV/c to the incoming charged particles as per the Lorentz Force law. The magnets provide information about the charge and momentum of the particles. They were operated at 2500 and 1800 amps respectively.

### Spectrometer tracks

In each event we reconstruct, on average, 12 - 15 high momentum tracks in the spectrometer. A spectrum of this measured momentum is shown in figure 2.3 . The measured momentum resolution for tracks which pass through the full spectrometer is given as

$$\frac{\delta p}{p} = 0.0047 + 0.00022 \times p(\text{GeV}/c) \quad . \quad [13] \quad (2.1)$$

## 2.4 Particle Identification

### Cherenkov Counters

There were two Cherenkov threshold detectors used by E791 for particle identification of pions, kaons and protons. C1 was filled with pure nitrogen and C2 was filled with a mixture of 80% helium and 20% nitrogen. Both the detectors were held at atmospheric pressure. Different threshold momenta for the above particle types in each counter are shown in the table 2.2. For any particle momentum we would expect to see light if it is above these thresholds. In this way a probability is formed based on the light

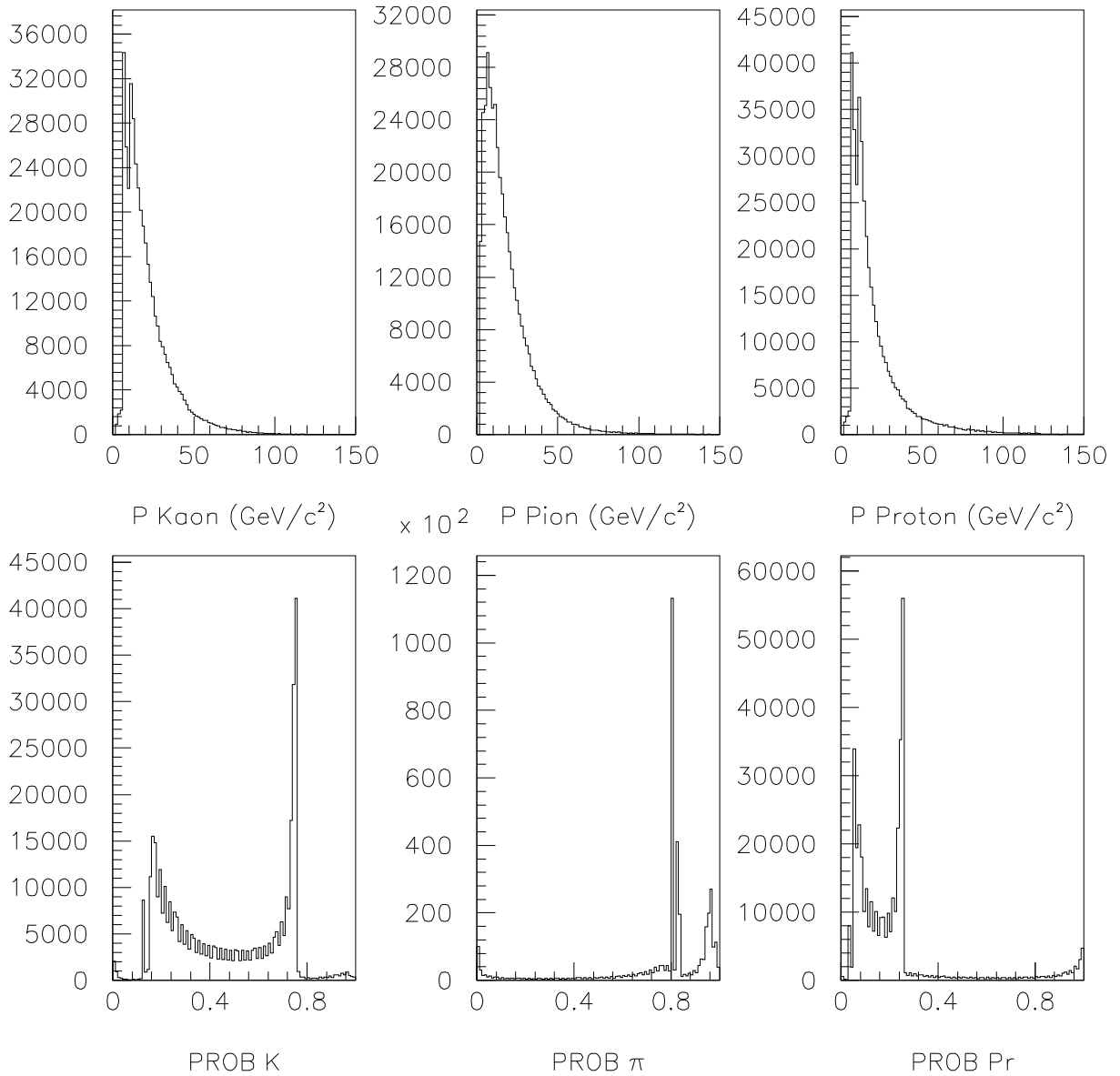


Figure 2.3: The momenta and the cherenkov probabilities of p, K and  $\pi$  on  $\Lambda_c \rightarrow pK\pi$  substrip.

seen in C1 and C2 for each particle type.  $\text{PROB}_\pi$ ,  $\text{PROB}_K$ ,  $\text{PROB}_p$  are displayed in (figure 2.3) for a set of spectrometer tracks.

### **SLIC and Hadrometer**

The segmented liquid Ionisation Calorimeter and the Hadrometer were used to measure the energy of the decay particles produced. The SLIC was designed to detect particles that primarily interact through electromagnetic processes. The Hadrometer can detect hadrons and help in muon detection. Both the detectors were also used in the experiment trigger.

### **Muon Walls**

Most of the particles are completely absorbed in the two calorimeters described above. Muons interact mainly through ionization and hence retain most of their energy after passing through the Calorimeters. These particles can be detected by simple scintillating paddles attached to phototubes.

E791 had two such muon scintillator arrays, 15X and 16Y, placed at the end of the spectrometer directly behind a 106cm thick steel shield wall for blocking the hadrons that had not ranged out in the calorimeters. These paddles gave the X and Y positions of muons at the rear of the spectrometer and indicated which tracks were muon candidates.

## **2.5 Data**

### **Trigger and Data Acquisition**

The goal of E791 was to collect a very large sample of charm particles. To accomplish this a loose trigger system was designed. The trigger required that a beam particle passed through the target and deposited an adequate amount of energy in the calorimeters, transverse to the beam direction. This transverse energy requirement is a mild indicator of a charm event being produced. The percentage of events accepted, the high beam rate, and the new data acquisition (DA) system increased the amount

of data collected by a factor of 5 over an earlier experiment E769.

The DA system needed to digitize and record data at an extremely high rate. The data arrived at a rate of 26Mbytes/sec during a Tevatron spill and was written to 42 Exabyte tapes (8mm) at a rate of 9Mbytes/sec. The data from the experimental detectors was read out by various methods like latches, analog-to-digital converters (ADCs), and to time-to-digital converters (TDCs).

During the process of writing, the data was compressed to allow more events to be written per tape. A typical 8mm Exabyte tape would contain about 800K events. Overall 24,000 data tapes were written which contain 20 billion events adding to 50Terabytes of data collected, the largest ever by a high energy particle physics experiment.

## 2.6 Farm Reconstruction

To accomplish the huge task of reconstructing this large charm sample, computer ‘farms’ were assembled at The University of Mississippi, Ohio State University (Currently at Kansas State University), Centro Brasileiro de Pesquisas Fisicas (Brazil) and Fermi Lab. The three US farms were composed of independent workstations linked through ethernet. The farm at the University of Mississippi[14] has 3000 MIPS (Million instructions per second) of computing power and the computing power at Kansas State matches our farm.

The Mississippi computers were Digital Equipment Corporation’s DEC station 5000s with fifty one 25, 33 and 40 MHz MIPS R3000 RISC CPU’s and seventeen 50MHz MIPS R4000 RISC cpus. The Ultrix operating system was used. The farm was divided by ethernet bridges into 4 servers each connected to a its own clients. The servers read out the data packets from the Exabyte tapes and send them to the clients. The clients, in turn, unpack the data, analyze the events using the E791 analysis package and write the selected and reconstructed events to a disk file. The

disk files were then written to Data Summary Tapes (DSTs). In this manner the farm operates as a loosely coupled parallel processing system.

The reconstruction of an entire run (set of 40 tapes) produces about 12-14 DSTs and takes about 35-40 hours. These DSTs are stripped and sent to the various collaborators on the experiment for further analysis and stripping. A weekly record of the farm reconstruction is shown below in figure 2.4

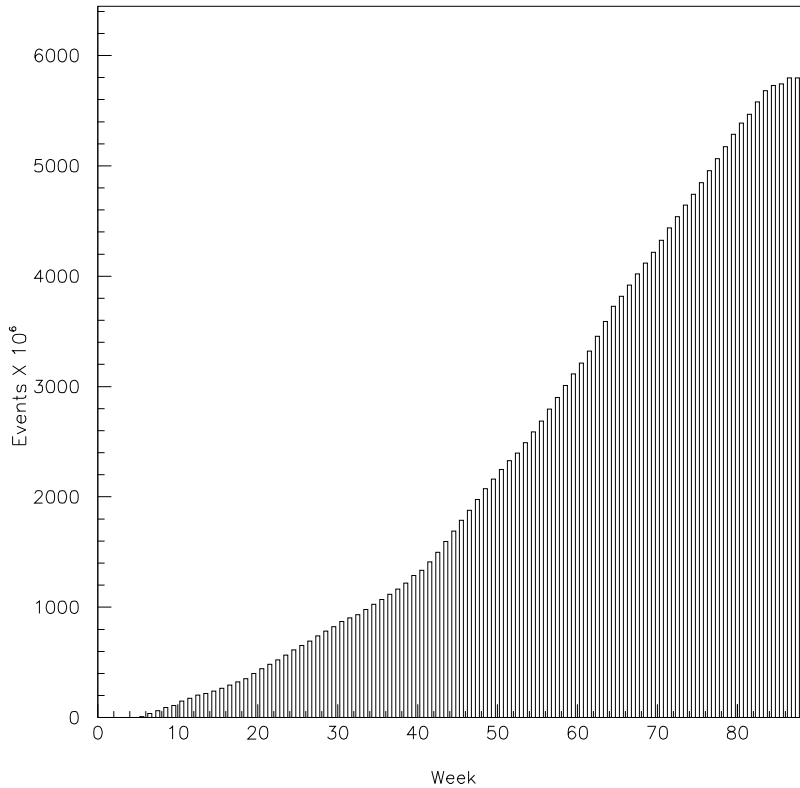


Figure 2.4: Cumulative number of events processed at Umiss starting November 1992 until July 1994.

### Monte Carlo Events

Monte Carlo events are man made events which simulate, through software, the charm production and spectrometer performance in detail. A charm particle is created, it decays, and all the tracks are propagated through the detector as in a real

event. An event record is written that is almost indistinguishable from a real data event. About 1 million  $\Lambda_c \rightarrow pK\pi$  events were generated for this analysis. They were processed through the farm reconstruction programs just like real data events.

### **Display of a Reconstructed Event**

In the figure 2.5 shown next page, a reconstructed event has been shown with the target region in grey. The location of the primary vertex and the secondary vertex are shown, with corresponding errors in grey ellipses. At the end of each track the track number, track category, momentum and the particle identification are recorded in that order from left to right. This may be a strong candidate for a  $D^+ \rightarrow K\pi\pi$ .

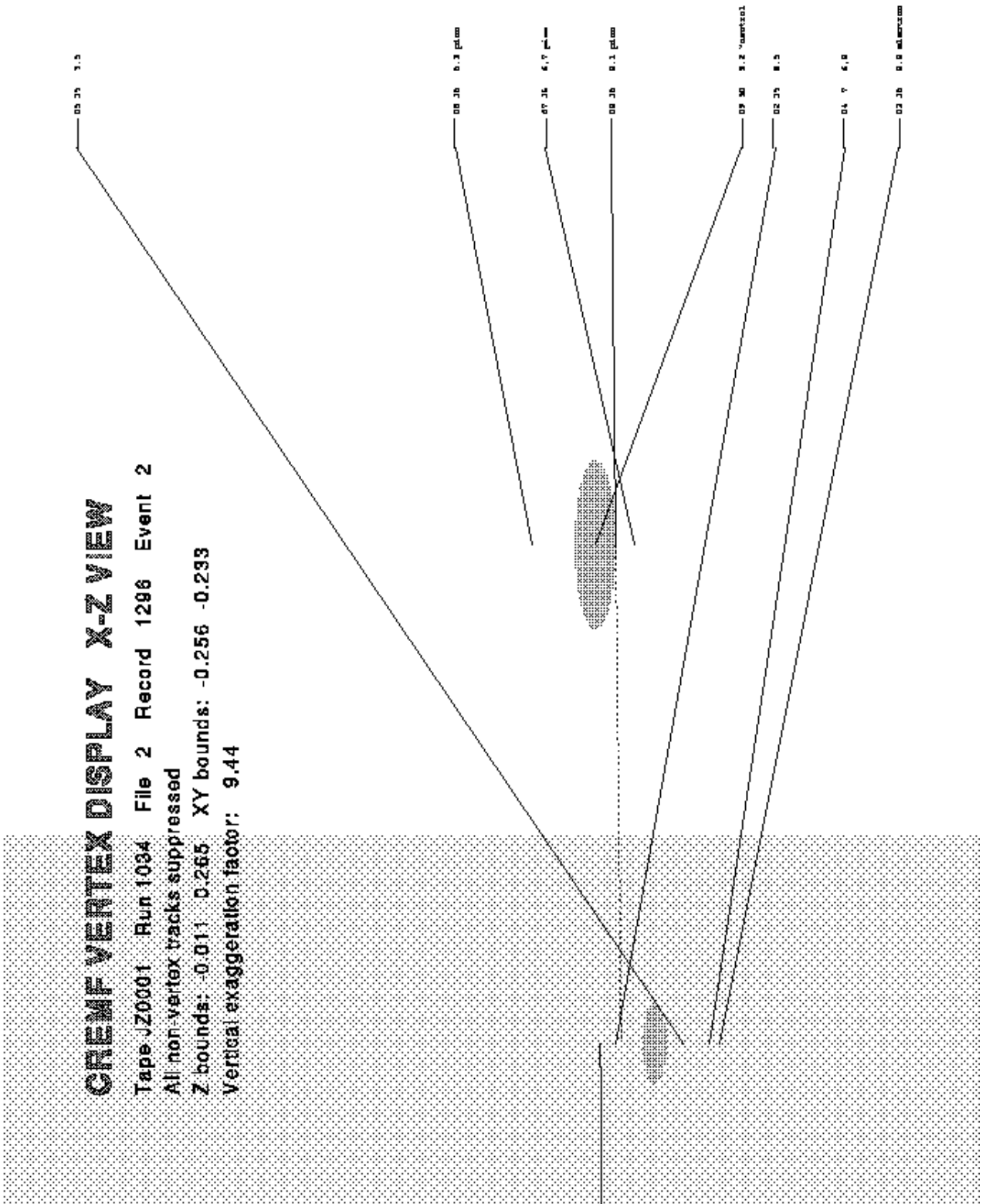


Figure 2.5: Display of a reconstructed event.

# Chapter 3

## Analysis of Data

### 3.1 Vertexing and Filtering of Events

The purpose of the analysis is to select charm events. In the first stage, probable charm events were filtered from the large data set by an algorithm which searches for charm decays, occurring just millimeters from the primary interaction. Spectrometer tracks are clustered into 3D vertices by a vertexing algorithm. Generally, most tracks, about 6, were put into the “primary vertex”, where the pion was thought to have interacted in a target. Tracks not belonging to this vertex were grouped into “secondary vertices”, where 2, 3 or greater “prongs” could form a vertex. Errors were taken into account in the vertex fitting. The end product was a list of vertex positions for each event and associated errors. About 15% of all the tracks were not put into a vertex but still kept for later analysis.

The farm reconstruction passed about 16% of the original event sample to the next level of analysis. Probable charm events were selected based on finding a secondary vertex downstream and well separated from the primary vertex. This selection criterion called the “Significance of Separation along the  $z$ -axis between the primary and the secondary vertices” (SDZ) is an important cut for distinguishing the charm particle decays from the background. Mathematically SDZ can be expressed as

$$SDZ = \frac{Z_{sec} - Z_{pri}}{\sqrt{\sigma_{pri}^2 + \sigma_{sec}^2}} = \frac{\Delta Z}{\sigma_Z}. \quad (3.1)$$

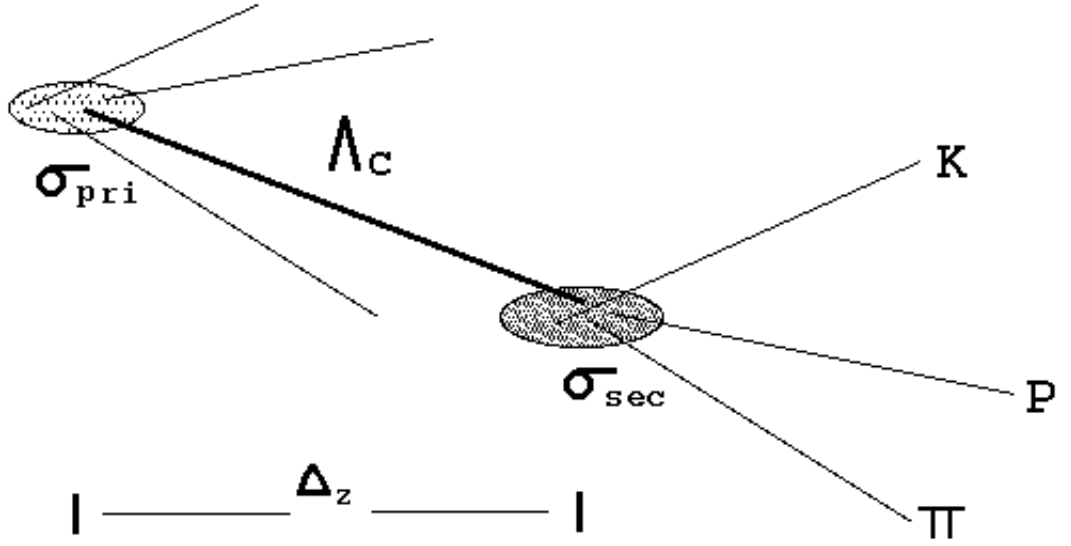


Figure 3.1: Illustration of SDZ.

$Z_{sec}$  and  $Z_{pri}$  are the positions of the secondary and primary vertices along the beam line respectively.  $\sigma_{pri}$  and  $\sigma_{sec}$  are the corresponding errors. At the filtering stage an  $SDZ \geq 4$  is applied or  $\Delta z \geq 4\sigma_z$  for three prongs. An illustration of a typical event with the “SDZ” cut is shown above. As the SDZ cut is increased the signal to noise ratio increases dramatically, but with loss in efficiency for detecting  $\Lambda_c \rightarrow pK\pi$ .

## 3.2 Stripping

Further processing of the Data Summary Tapes is called “stripping”. Stripping involves more selective analysis of data on the DSTs and reduces the number of events needed to be handled in further analyses. We used a Vertex-list driven approach where each event is examined by looking at the vertices formed by the intersection of two or more particle tracks in the vertex list as described above. We were searching for events that had a well separated secondary vertex, that contained 3 tracks, and in  $\Lambda_c \rightarrow pK\pi$  decays, two of the tracks must be identified as a proton and a kaon. Two strips were applied to events passing the filter stage. First an N-prong strip and then a specific  $pK\pi$  analysis strip.

## Nprong Strip

A total of 364 runs were processed through the Nprong strip. The Nprong strip passed all events that had one secondary vertex with 3 or greater number of tracks. One of the tracks must be a strong proton or a kaon candidate. This strip will save all events like  $\Lambda_c \rightarrow pK\pi$ ,  $D_s^+ \rightarrow KK\pi$ , and  $D^s \rightarrow K\pi\pi$ . The  $D_s^+$  and  $D^+$  are very similar to  $\Lambda_c \rightarrow pK\pi$  and were kept for background studies. Each run of about 32 million events was reduced to about 900k events by the Nprong strip.

## pK $\pi$ Analysis Strip

The  $\Lambda_c \rightarrow pK\pi$  strip looks specifically for this mode. The  $\Lambda_c \rightarrow pK\pi$  substrip loops over all the secondary vertices and picks the vertices with exactly 3 tracks (prongs). The total summed charge ( $q_{tot}$ ) must be  $\pm 1$  imposing the conservation of charge condition.<sup>1</sup> Since the kaon will always have the sign that is opposite to that of the  $\Lambda_c$ , the track with this sign is assigned to a kaon. The other two tracks are assigned to the proton and the pion. Now, for these two tracks, the probability of these being a proton is computed using the cherenkov probabilities and the track with higher probability is marked as a proton and the remaining track would be the pion. On the track that is assigned for the kaon a cherenkov kaon identification cut ( $PROB_K > 0.15$ ) is applied. All track combinations satisfying the above criteria are stored. Mass and cherenkov proton identification cut ( $PROB_p > 0.05$ ), a very loose cut, are applied to them. For all those vertices that pass through these cuts the Lorentz invariant mass (Equation 3.2) of the  $pK\pi$  candidate is computed by adding the masses of the tracks in the vertex,

$$M_{pK\pi}^2 = (E_p + E_K + E_\pi)^2 - (P_p + P_K + P_\pi)^2. \quad (3.2)$$

The resultant  $\Lambda_c$  candidate mass  $M_{pK\pi}$  is subjected to a mass window cut requiring that the  $M_{pK\pi}$  mass should be greater than 2.1GeV/ $c^2$  and less than 2.5 GeV/ $c^2$  to reduce the data sample.

All the vertices that pass through the mass window cut are accepted and are subjected to further tests or cuts. The cuts are defined as follows:

---

<sup>1</sup>The decay of  $\Lambda_c^\pm$  will be  $\Lambda_c^+ \rightarrow p^+ K^- \pi^+$  and  $\Lambda_c^- \rightarrow p^- K^+ \pi^-$ .

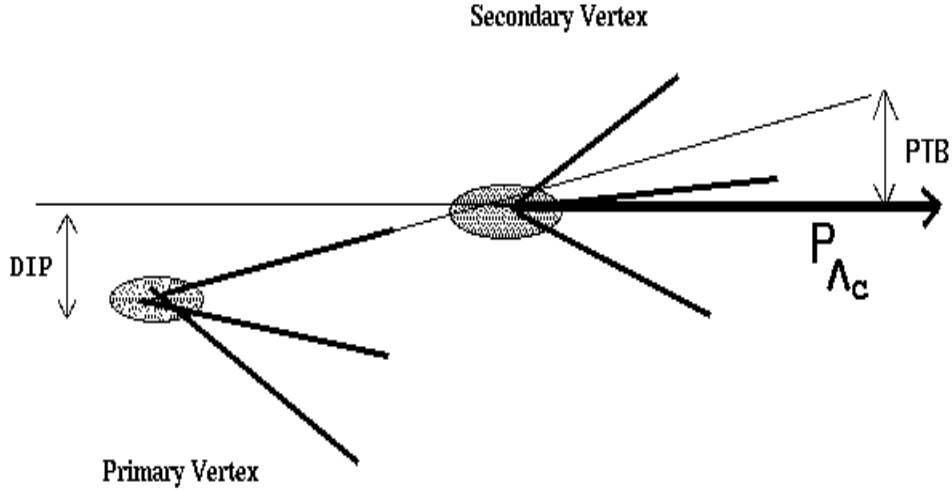


Figure 3.2: Illustration of the DIP and PTB cuts.

1. SDZ: Significance of separation of primary and secondary vertices discussed above.
2. PTB: Transverse momentum balance about the  $\Lambda_c$  line of flight. This parameter checks for the conservation of momentum of the  $\Lambda_c$  candidate and the  $pK\pi$  candidates.
3. DIP: Impact parameter of the  $\Lambda_c$  momentum vector at the primary vertex. The resultant momentum of the three tracks ( $pK\pi$ ) from the secondary vertex, when projected backwards should point to the primary vertex, and an estimate of the error is called the DIP as shown in the figure (3.2) above.
4. TAU: Proper lifetime cut for the particle. Typically a  $\Lambda_c$  particle lives for 0.20ps. We can utilise this information and place an upper limit on the proper lifetime of the candidate.  $\tau < 1.3$  picosecs. Decays beyond this time are likely to be background or other charm decays. The proper life time of the particle is computed using the expression

$$\tau = \frac{l}{c\beta\gamma}.$$

5. CHVTX: The chi square of the fitted secondary vertex. This cut selects good vertex candidates.
6.  $\text{PROB}_\pi, \text{PROB}_K, \text{PROB}_p$ :  $\pi, K, p$  probabilities determined by the cherenkov light detectors (discussed in chapter 2, refer to figure 2.2 for the spectrum of Cherenkov probabilities)

These parameters are plotted and shown in the figure 3.3. The cuts applied at this stage are very mild. The events filtered by this strip are written to Data Tapes which go through another process of stripping. The stripping at this point is done in two different ways. The programs search for probable  $\Lambda_c$  and  $\Sigma_c$  candidates and write them to a disk file. Various parameters pertaining to the track, particle properties are written to the disk file to facilitate detailed analysis and proper selection of the final cuts. A list of cuts used at several stages of analysis are given in table 3.1.

Cut	NPRONG	STRIP	$\Lambda_c \rightarrow$ ANALYSIS	$\Sigma_c \rightarrow$ ANALYSIS
NPRONG	$\geq 3$	3	3	
SDZ >	4	4	10	6
PTB <	0.50GeV/c		0.35 GeV/c	0.50 GeV/c
CHVTX <			5	
TAU <	1.5ps			
DIP <	120 $\mu$ m			
PROB $_{\pi}$ >		0.1	0.1	
PROB $_K$ >	0.13			
PROB $_p$ >	0.12			
PROB $_{pk\pi}$ >		0.1	0.1	0.2
INPRI				1

Table 3.1: Summary of cuts used at several stages of analysis

### Monte Carlo Events and Selection of Cuts

About a million E791 Monte Carlo Events were generated and were passed through the same stripping process as the real data. These Monte Carlo events aid us in selecting efficient cuts to apply to the real data. The Monte Carlo events were also used for calculating the efficiencies pertaining to the  $X_F$  distribution or other distributions. Below we show the spectrometer efficiency for reconstructing  $\Lambda_c \rightarrow pK\pi$  decays as a function of  $X_F$ , figure 3.4. We also show a comparison of Monte Carlo and Data Events in figures 3.5 and 3.6 Cuts were selected based on optimising the Monte Carlo signal relative to background in the data, so as not to bias selection of  $\Lambda_c$  events.

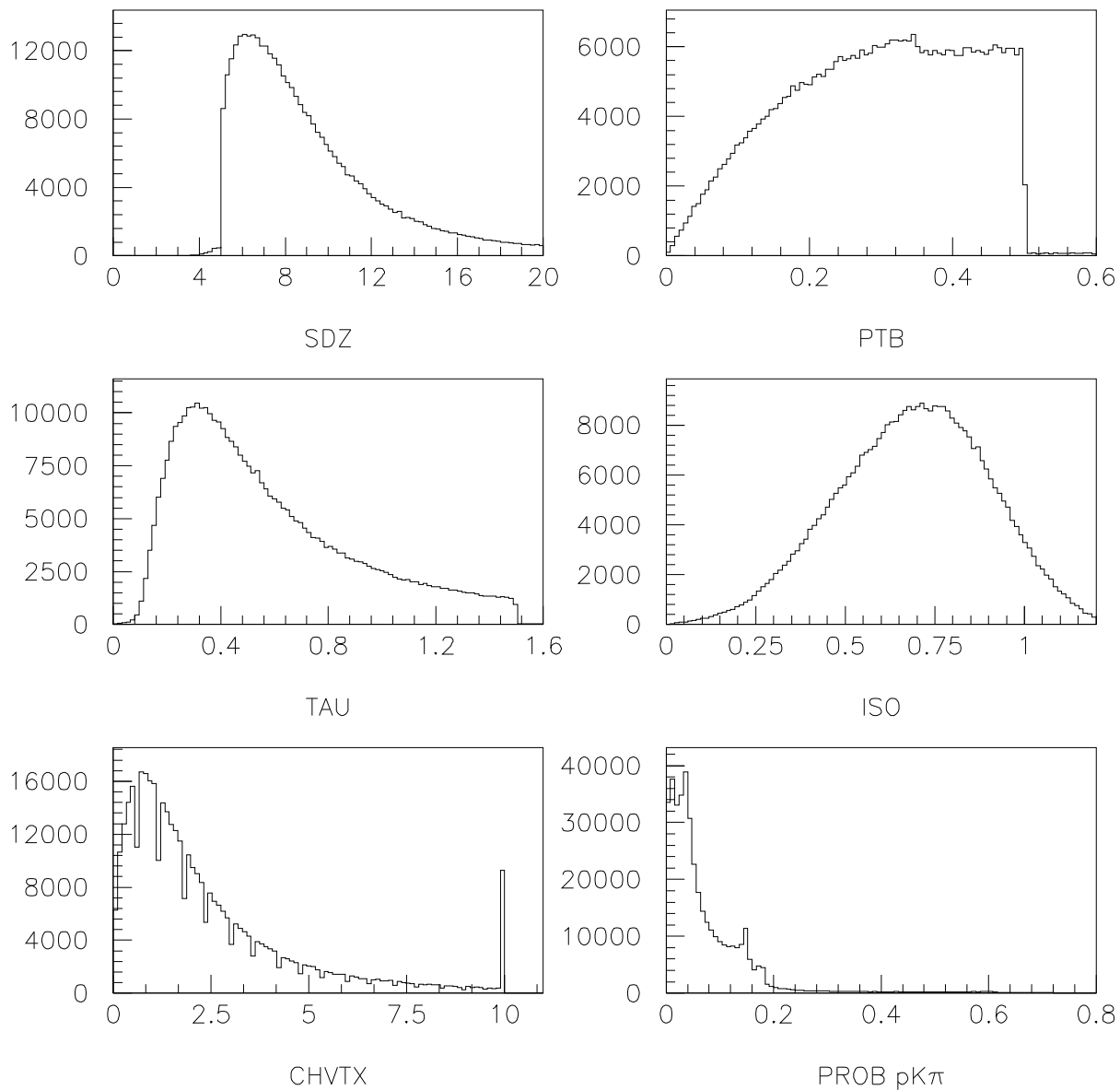


Figure 3.3: The spectra of selection parameters for the vertices and tracks from data collected on the final substrip.

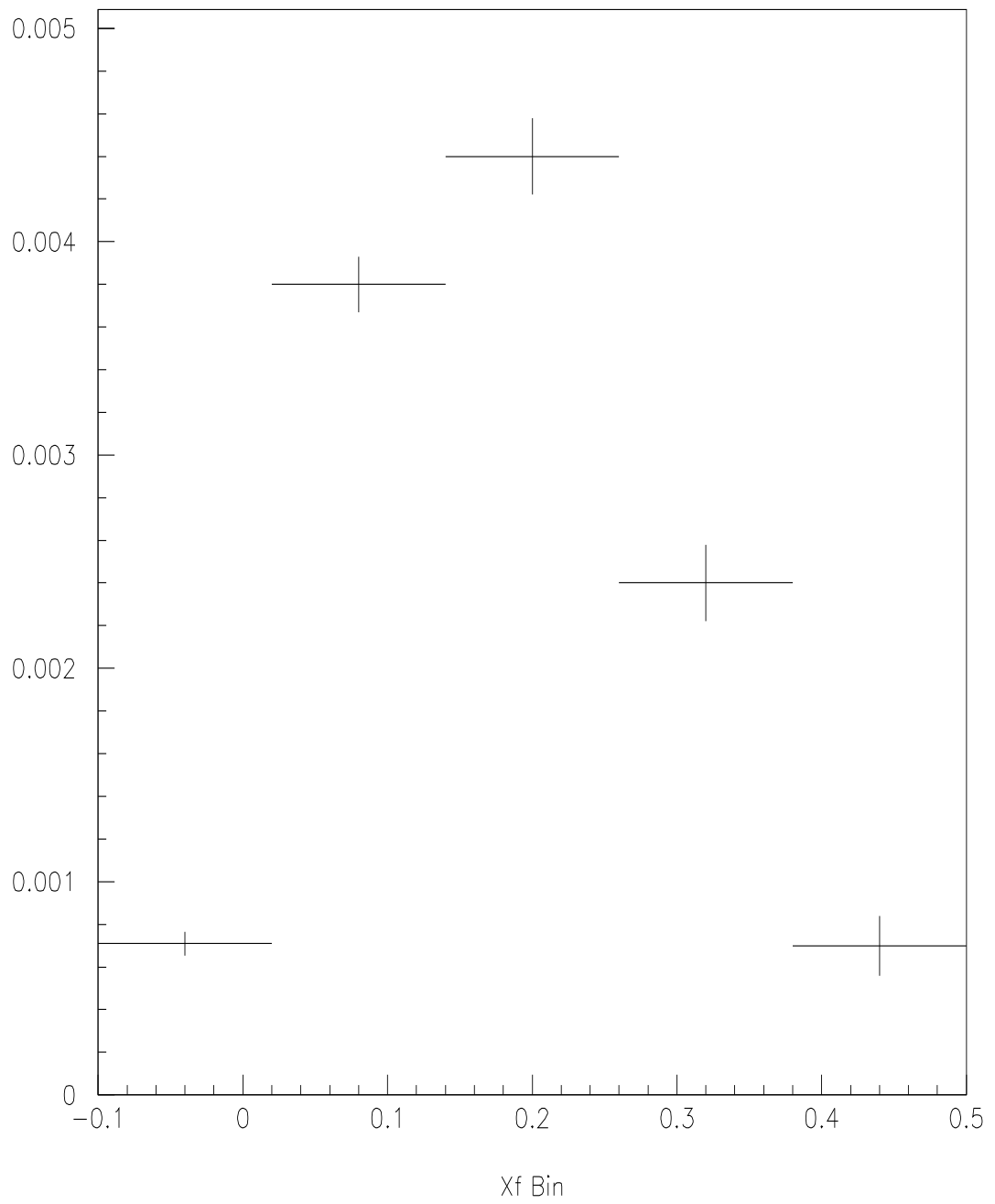


Figure 3.4: Detector efficiency vs  $X_F$  determined from Monte Carlo events.

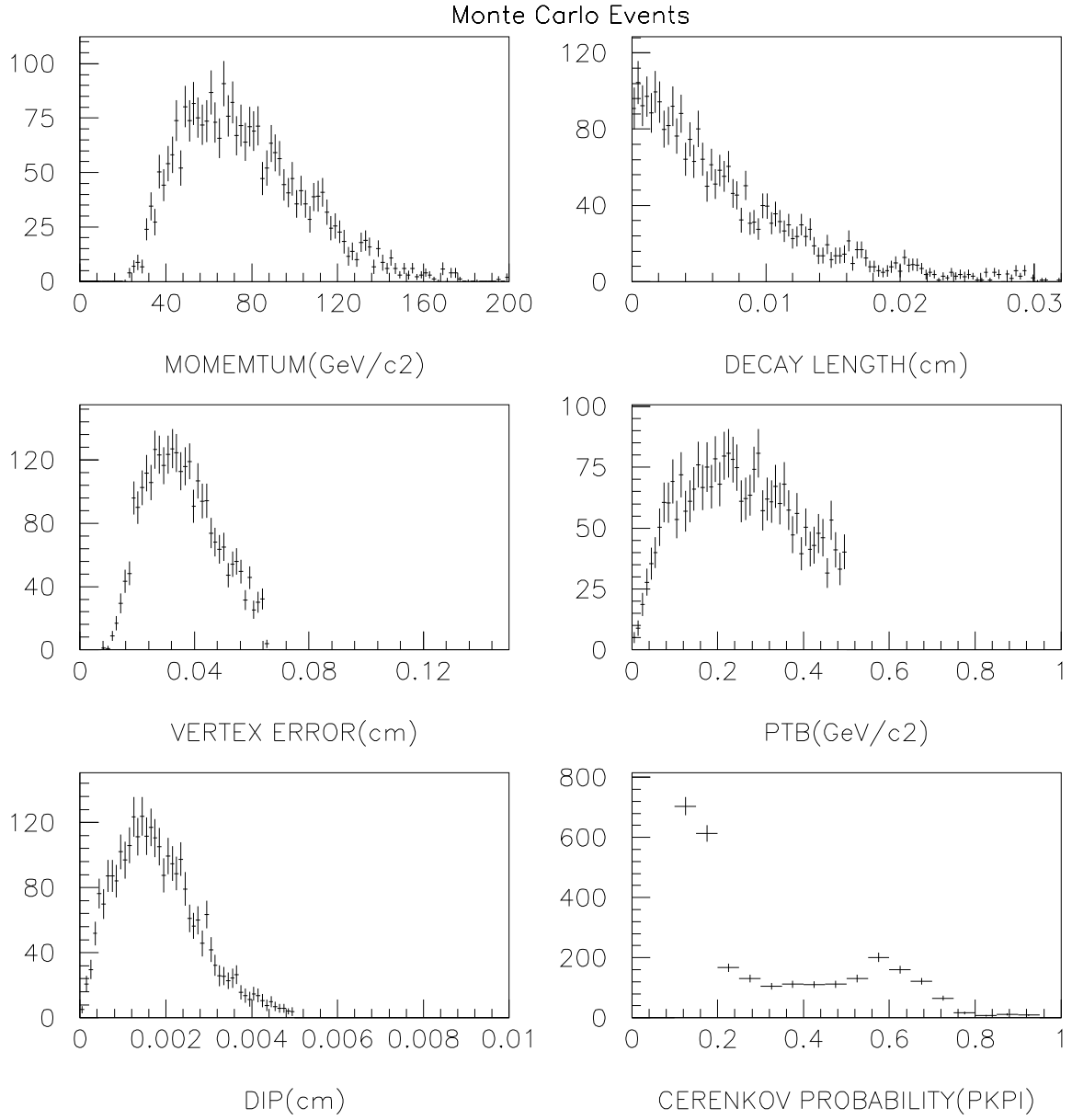


Figure 3.5: Some distributions found in Monte Carlo events.

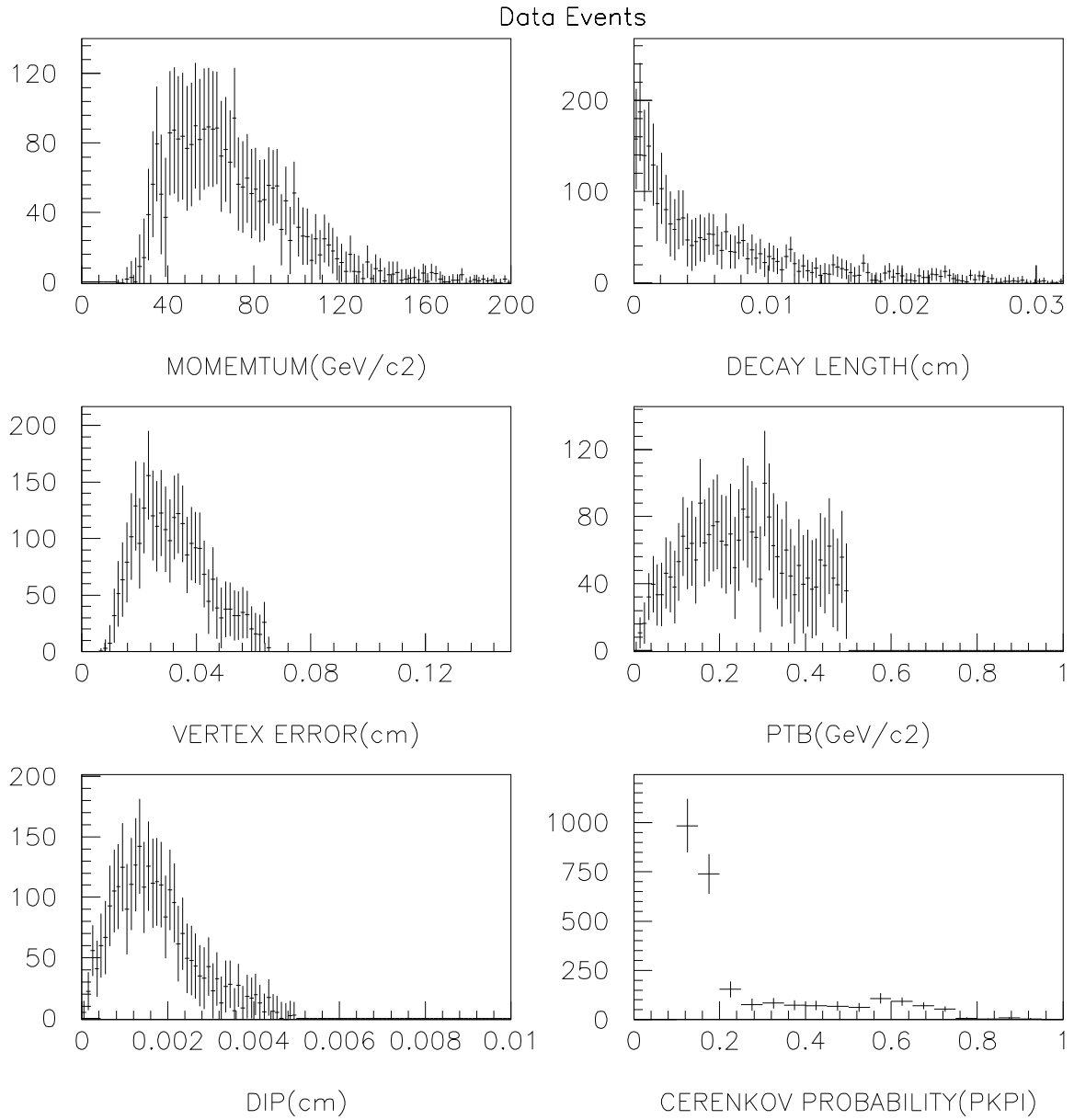


Figure 3.6: Some distributions found in data events.

### 3.3 Analysis

#### $\Lambda_c \rightarrow \text{pK}\pi$ Signal Analysis

The substripped events are passed through another step of filtering to further reduce the size of the data before being written to a disk file. This file is then loaded on to the Physics Analysis Workstation (PAW) Histogramming package and the final cuts are selected and fitting analysis performed. A list of final cuts applied are shown in the table above along with cuts from previous filters.  $\text{PROB}_{\text{pK}\pi}$  is the product of the cherenkov probabilities for the p,K and  $\pi$  candidates.

The final  $\Lambda_c$  mass spectrum is shown in figure 3.7. A gaussian fit to the  $\Lambda_c$  signal and linear fit to the background gives  $982 \pm 52$   $\Lambda_c \rightarrow \text{pK}\pi$  events. Table 3.2 shows the number of  $\Lambda_c$ 's found and their mean measured masses. We make an estimate of the total cross-section in chapter 4.

The measured ratio of  $\Lambda_c^+$  to  $\Lambda_c^-$  is

$$\frac{N_{\Lambda_c^+}}{N_{\Lambda_c^-}} = \frac{523 \pm 35}{459 \pm 37} = 1.14 \pm 0.12. \quad (3.3)$$

This corresponds to a small enhancement of  $\Lambda_c^+$  to  $\Lambda_c^-$  as mentioned in chapter 1. If we assume the efficiency for reconstructing  $\Lambda_c^+ D^-$  and  $\Lambda_c^+ \Lambda_c^-$  events are about the same,  $\epsilon_1 \simeq \epsilon_2$ , using equation 1.7, we obtain

$$\frac{\sigma_{\Lambda_c^+ D^-}}{\sigma_{\Lambda_c^+ \Lambda_c^-}} \simeq 0.14 \pm 0.12. \quad (3.4)$$

The ratio suggests that most  $\Lambda_c$ 's are produced by a symmetric production mechanism. The contribution from diquark fragmentation is small.

E791 also measured the ratio of  $D^-$  to  $D^+$  mesons[15].

$$\frac{N_{D^-}}{N_{D^+}} = 1.22 \pm 0.01 \quad (3.5)$$

The ratios (3.3) and (3.5) are consistent with each other, although the  $D^-$  to  $D^+$  ratio is determined with much higher accuracy. Ratio 3.5 also suggests that the associated production mechanism contributes about 20% to the total production of  $\Lambda_c^+$  and  $D^-$ .

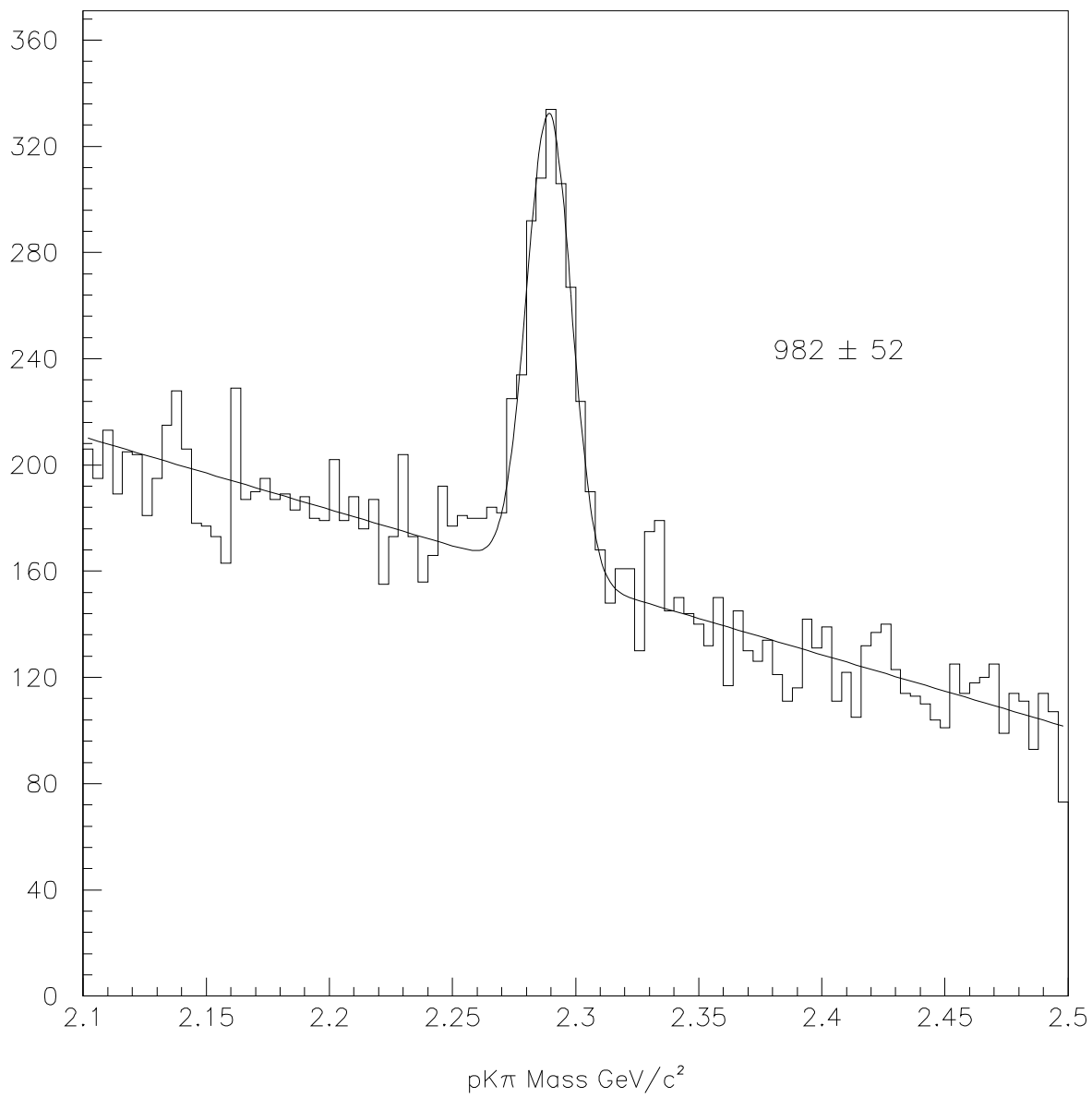


Figure 3.7: The  $M_{pK\pi}$  fitted mass spectrum.

	$\Lambda_c^\pm$	$\Lambda_c^+$	$\Lambda_c^-$
$N_{\Lambda_c}^{obs}$	$982 \pm 52$	$523 \pm 35$	$459 \pm 37$
M (GeV/c <sup>2</sup> )	$2.289 \pm 0.00025$	$2.290 \pm 0.00058$	$2.289 \pm 0.00066$

Table 3.2: Number of observed  $\Lambda_c \rightarrow pK\pi$  events and fitted mass differences

### $X_F$ Analysis

The Feynman  $X$  spectrum of  $\Lambda_c$  particles was extracted by dividing the  $pK\pi$  candidates into several  $X_F$  ranges. The resultant mass plots were then fit to a gaussian signal component and linear background giving  $N^{obs}$  for each bin of  $X_F$ . The width of the  $\Lambda_c$  signal was fixed to 8 MeV/c<sup>2</sup> in these fits.

$X_F$ Bin	$N_{mc}^{obs} \pm \sigma_N$	$N_{mc}^{gen}$	$\epsilon = N_{mc}^{obs}/N_{mc}^{gen}$	$N^{obs}$	$N(X)$
-0.1 - 0.0	$138 \pm 11$	195305	$7.1E^{-4} \pm 5.6E^{-5}$	$105 \pm 18$	$14872 \pm 2809$
0.0 - 0.1	$797 \pm 27$	210219	$3.8E^{-3} \pm 1.3E^{-4}$	$472 \pm 34$	$124868 \pm 9967$
0.1 - 0.2	$683 \pm 28$	154458	$4.4E^{-3} \pm 1.8E^{-4}$	$323 \pm 28$	$73077 \pm 6999$
0.2 - 0.3	$218 \pm 16$	89987	$2.4E^{-3} \pm 1.8E^{-4}$	$64 \pm 11$	$27083 \pm 5078$
0.3 - 0.4	$30 \pm 6$	42030	$7.1E^{-4} \pm 1.4E^{-4}$	$20 \pm 6$	$28011 \pm 10039$

Table 3.3:  $X_F$  analysis  $\Lambda_c^\pm$ .

The true number of  $\Lambda_c$  in that range is  $N(X) = N^{obs}(X)/\epsilon_x$  where  $\epsilon_x$  is the efficiency for detection in that  $X_F$  bin. We define

$$\epsilon_x = \frac{N_{mc}^{obs}(X)}{N_{mc}^{gen}(X)} \quad (3.6)$$

as the ratio of the number of reconstructed Monte Carlo events to generated events in each  $X_F$  range. I show the  $X_F$  spectrum of  $\Lambda_c$ 's in figure 3.8 . If we fit this spectrum to a form  $\frac{dN}{dX_F} = (1 - |X_F|)^n$ , for  $0.0 \leq X_f \leq 0.4$ , we get a value  $n = 5.8 \pm 0.6$  .

### $\Sigma_c \rightarrow \Lambda_c \pi$ Analysis

The  $\Sigma_c$  decays strongly to  $\Lambda_c \pi$ . The pion is required to come from the primary vertex list, signified by INPRI = 1 in the table, and the  $\Lambda_c \rightarrow pK\pi$  in a 3 prong

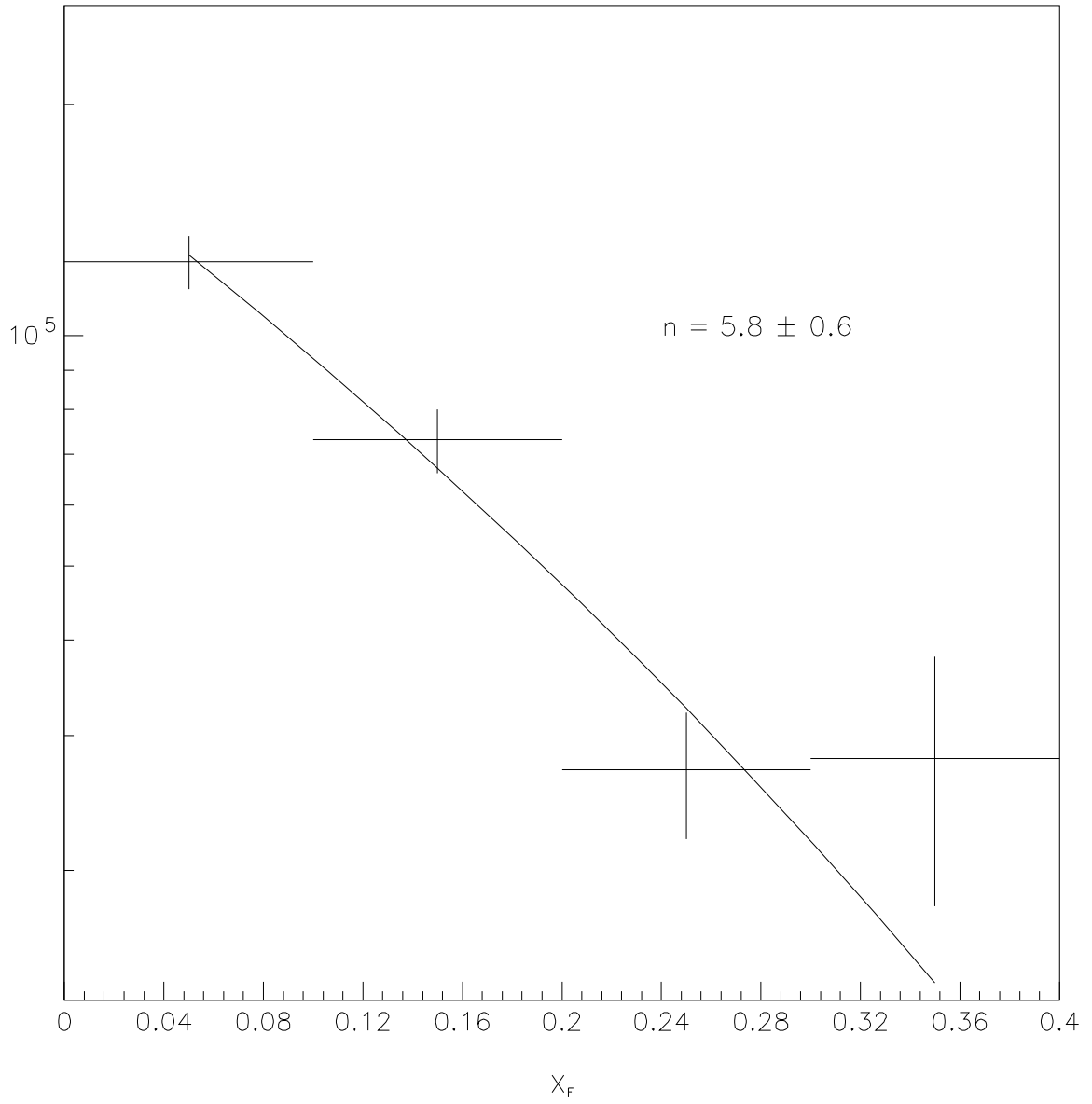


Figure 3.8: Acceptance corrected  $X_F$  spectrum fitted to  $\frac{dN}{dX_F} = (1 - |X_F|)^n$ .

secondary vertex as usual. Events which are selected by the earlier substrip are taken and an additional loop over the tracks from the primary vertex is added, looking for the signature of a pion. Once this additional track is found, the invariant mass of the  $\Lambda_c\pi$  combination is calculated and the  $\Sigma_c$  mass is computed. The SDZ cut has been lowered to a significance factor of 6 and the cherenkov product probability  $\text{PROB}_{pK\pi}$  is raised to 0.2 with the other cuts remaining the same. The list of cuts shown for this analysis is shown in table 3.1.

The mass difference spectrum of the  $\Sigma_c$  and  $\Lambda_c$  candidates ( $\Delta M$ ) should start at the pion mass and rise slowly. The  $\Sigma_c$  will emerge as a peak over this rising background.

$$\Delta M = M_{pK\pi\pi} - M_{pK\pi} \quad (3.7)$$

It is also required that  $\Delta M$  should be less than  $0.280\text{GeV}/c^2$  to reduce the size of the data sample. The charge of the four tracks ( $p, K, \pi$  from the secondary vertex and the  $\pi$  from the primary vertex) are added and written to the disk file to distinguish  $\Sigma_c^{++}$  and  $\Sigma_c^0$  decays.

	$\Sigma_c^{tot}$	$\Sigma_c^0$	$\Sigma_c^{++}$
$N_{\Sigma_c}^{obs}$	$76 \pm 14$	$53 \pm 11$	$23 \pm 9$
$\Delta M$ (MeV/c <sup>2</sup> )	$166.5 \pm 5$	$166.7 \pm 7$	

Table 3.4: Number of observed  $\Sigma_c$  and fitted masses(MeV/c<sup>2</sup>).

The  $\Delta M$  mass plots for the  $\Sigma_c^0, \Sigma_c^{++}$ , and total  $\Sigma_c^{0,++}$  are shown in figure 3.9. A fit to a gaussian signal and quadratic background is displayed. The width of the gaussian is fixed to  $4\text{MeV}/c^2$  based on the Monte Carlo data. The fit results are given in table 3.4. The plots of the  $\Delta M$  spectrum are shown in figure 3.9 .

An estimate of the ratio of the number of  $\Sigma_c$ 's to all  $\Lambda_c$ 's produced can be made following equation (1.8). The production ratio of the can be expressed as

$$\frac{N_{\Sigma_c}}{N_{\Lambda_c}} = \frac{N_{\Sigma_c}^{obs}}{N_{\Lambda_c}^{obs}} \times \frac{\epsilon_{pK\pi}}{\epsilon_{pK\pi\pi}} = \frac{N_{\Sigma_c}^{obs}}{N_{\Lambda_c}^{obs}} \times \frac{1}{\epsilon_\pi} \quad (3.8)$$

We have expressed  $\epsilon_{pK\pi\pi} = \epsilon_{pK\pi} \times \epsilon_\pi$ , where  $\epsilon_{pK\pi}$  is the efficiency for reconstructing

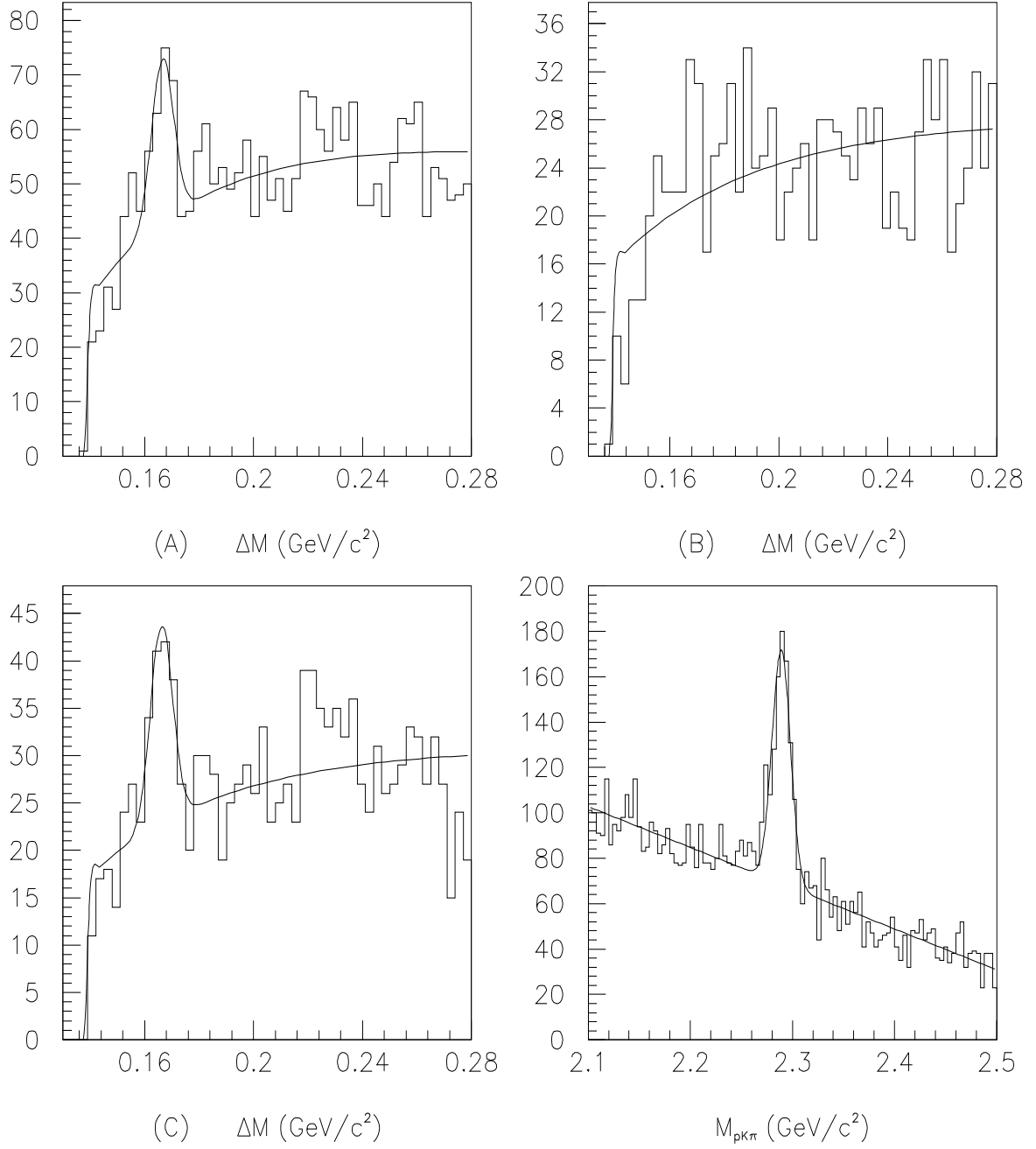


Figure 3.9:  $\Sigma_c$  fitted mass plots: (A)  $\Sigma_c$  sum plot (B)  $\Sigma_c^{++}$  plot (C)  $\Sigma_c^0$  plot and  $M_{\Lambda_c \rightarrow p K \pi}$  plot with  $\text{SDZ} > 6$ ,  $\text{PTB} < 0.50 \text{ GeV}/c$  and  $\text{PROB}_{p K \pi} > 0.20$ .

$\Lambda_c \rightarrow pK\pi$  and the  $\epsilon_\pi$  is the efficiency for reconstructing the pion in the primary vertex. The observed number of  $\Lambda_c \rightarrow pK\pi$  with  $SDZ > 6$ ,  $PTB < 0.50$  GeV/c and  $PROB_{pK\pi} > 0.2$  is  $N_{\Lambda_c}^{obs} = 722 \pm 43$ . We estimate  $\epsilon_\pi = 0.76 \pm 0.08$  from other Monte Carlo data [16]. Finally we get a ratio of

$$\frac{N_{\Sigma_c^0}}{N_{\Lambda_c}} = \frac{53 \pm 11}{722 \pm 43} \times \frac{1}{0.76 \pm 0.08} = 0.09 \pm 0.022 \quad . \quad (3.9)$$

A similar calculation of the ratio  $N_{\Sigma_c^{++}}$  to  $N_{\Lambda_c}$  gives

$$\frac{N_{\Sigma_c^{++}}}{N_{\Lambda_c}} = 0.04 \pm 0.016 \quad (3.10)$$

### $\Lambda_c \rightarrow pK^{*0}(890)$ Analysis

A larger fraction of  $\Lambda_c \rightarrow pK\pi$  decays proceed through  $pK^{*0}$ . In the analysis strip for  $\Lambda_c \rightarrow pK\pi$ , the two-body masses  $M_{K\pi}$ ,  $M_{p\pi}$  and  $M_{Kp}$  are computed. A Dalitz plot of  $M_{K\pi}^2$  vs  $M_{p\pi}^2$  for events such that  $M_{pK\pi}$  is in mass range  $2.26 \leq M_{pK\pi} \leq 2.32$  GeV/c<sup>2</sup> has been plotted and shown in figure 3.10. This plot indicates a strong resonance on the  $M_{K\pi}^2$  axis at a mass  $M_{K\pi}^2 \simeq [0.89 \text{ GeV}/c^2]^2$ , the  $K^{*0}(890)$ . No other resonance structure is obvious. This Dalitz plot contains both signal and background events.

We estimate the number of  $pK^{*0}$  decays relative to all  $pK\pi$  decays by directly fitting the  $pK\pi$  mass plot with a  $K^{*0}$  constraint. We show the  $M_{K\pi}$  plot for events in the above  $M_{pK\pi}$  mass region in figure 3.12. Looking for the  $K\pi$  events in the signal region of the  $\Lambda_c$   $2.26 \leq M_{pK\pi} \leq 2.32$  GeV/c<sup>2</sup> shows a peak over a linear background which corresponds to the  $K^{*0}$  resonance. This peak spans a mass range of  $0.84 \leq M_{K\pi} \leq 0.94$  GeV/c<sup>2</sup>.

Imposing the above  $M_{K\pi}$  mass range cut on all the  $\Lambda_c \rightarrow pK\pi$  events approximately gives the number of  $\Lambda_c$  events decaying through the  $K^{*0}$  resonance. This  $M_{pK\pi}$  mass plot is shown in figure 3.11. Fitting the plot we obtain  $N_{pK^{*0}}^{obs} = 281 \pm 25$  events. We calculate the relative branching ratio for the  $pK^{*0}$  resonance using the expression

$$\frac{BR(\Lambda_c \rightarrow pK^{*0})}{BR(\Lambda_c \rightarrow pK\pi)} = \frac{N_{\Lambda_c \rightarrow pK^{*0}}^{obs}}{N_{\Lambda_c \rightarrow pK\pi}^{obs}} \times \frac{\epsilon_{\Lambda_c \rightarrow pK\pi}}{\epsilon_{\Lambda_c \rightarrow pK^{*0}}} \times \frac{1}{BR(K^{*0} \rightarrow K\pi)} \quad (3.11)$$

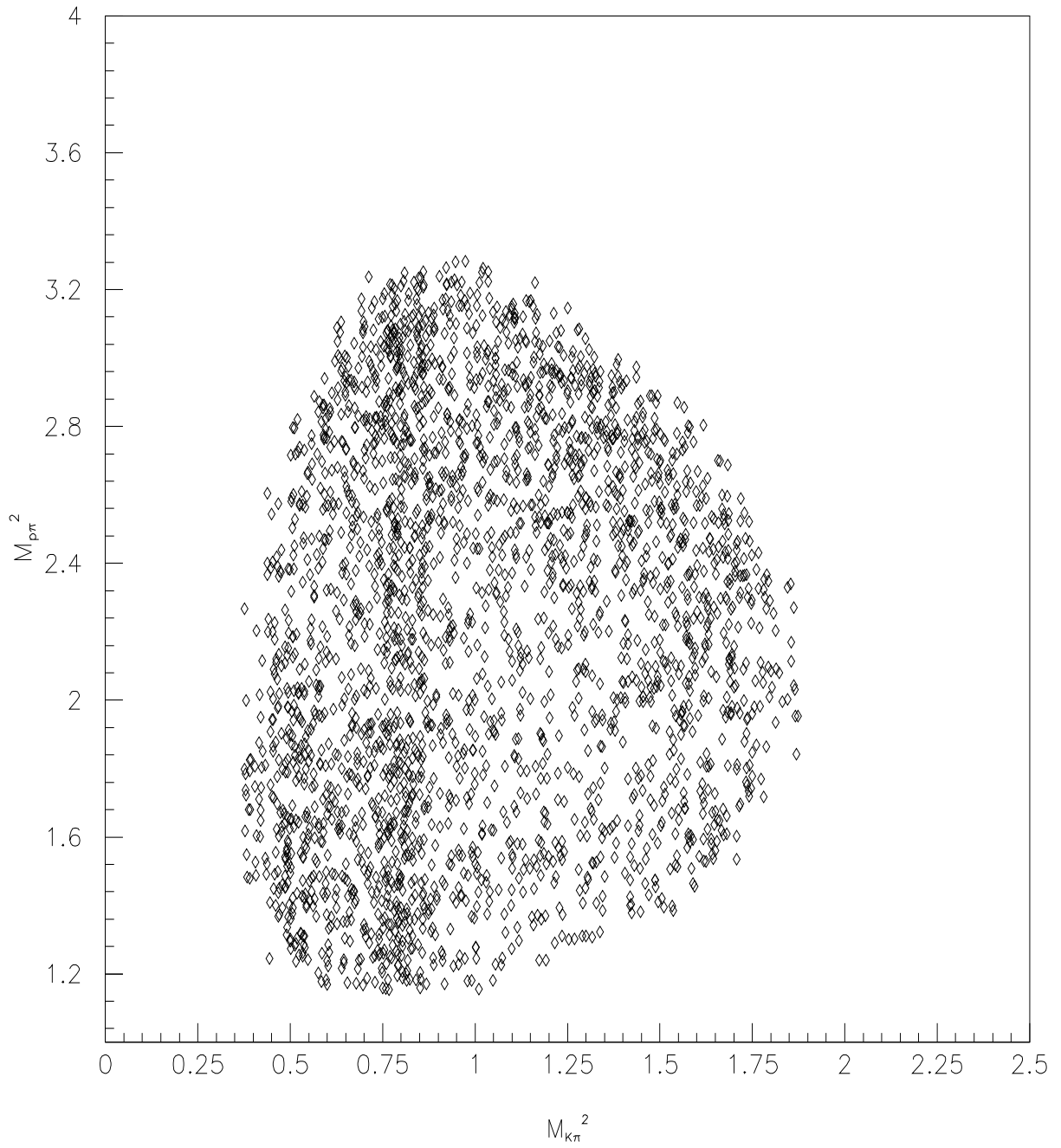


Figure 3.10: Dalitz plot  $M_{K\pi}^2$  vs  $M_{p\pi}^2$  ( $\text{GeV}/c^2$ )<sup>2</sup>.

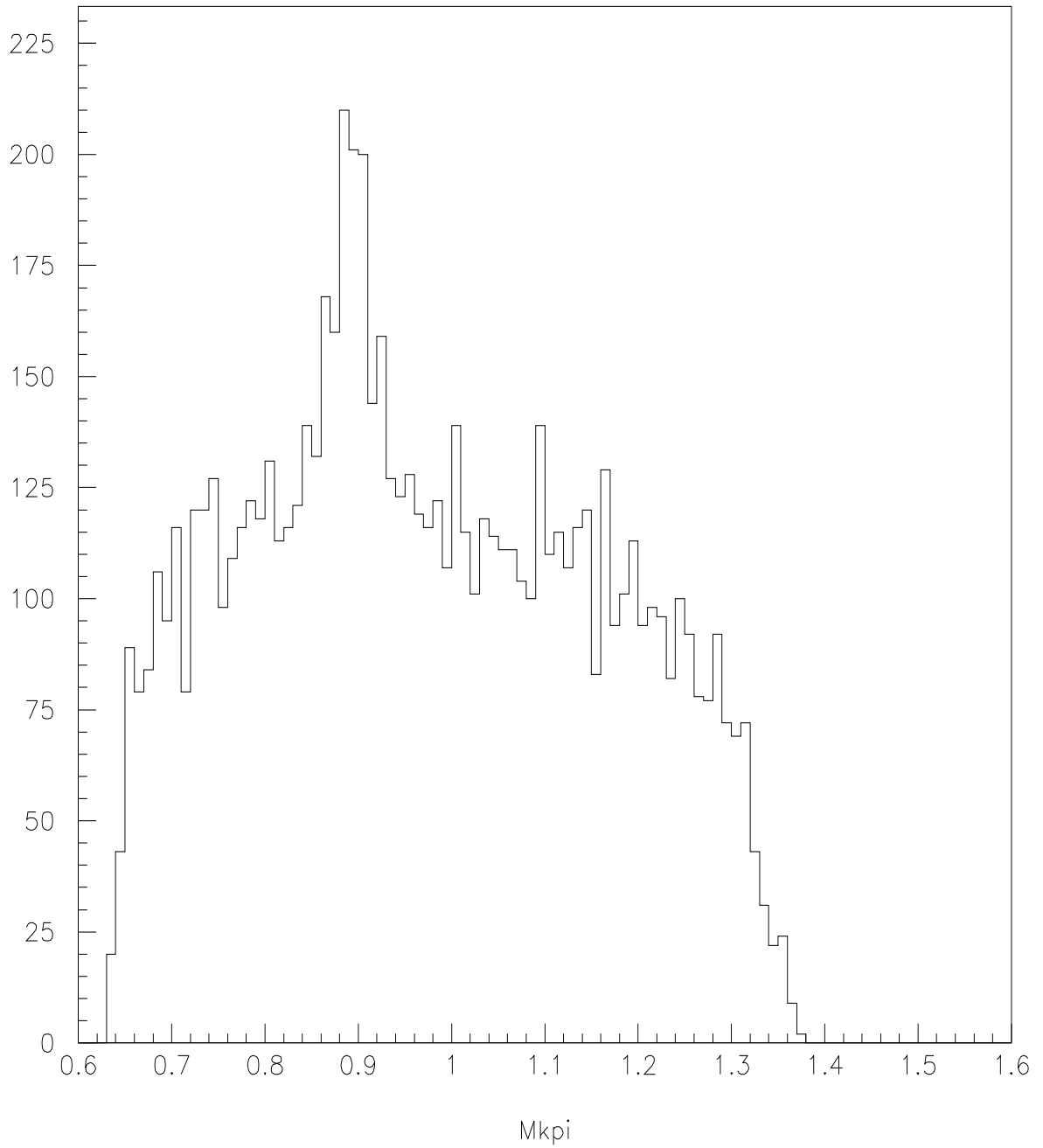


Figure 3.11: The  $M_{K\pi}$  spectrum from all  $\Lambda_c$  events,  $2.26 \leq M_{pK\pi} \leq 2.32$  ( $\text{GeV}/c^2$ ).

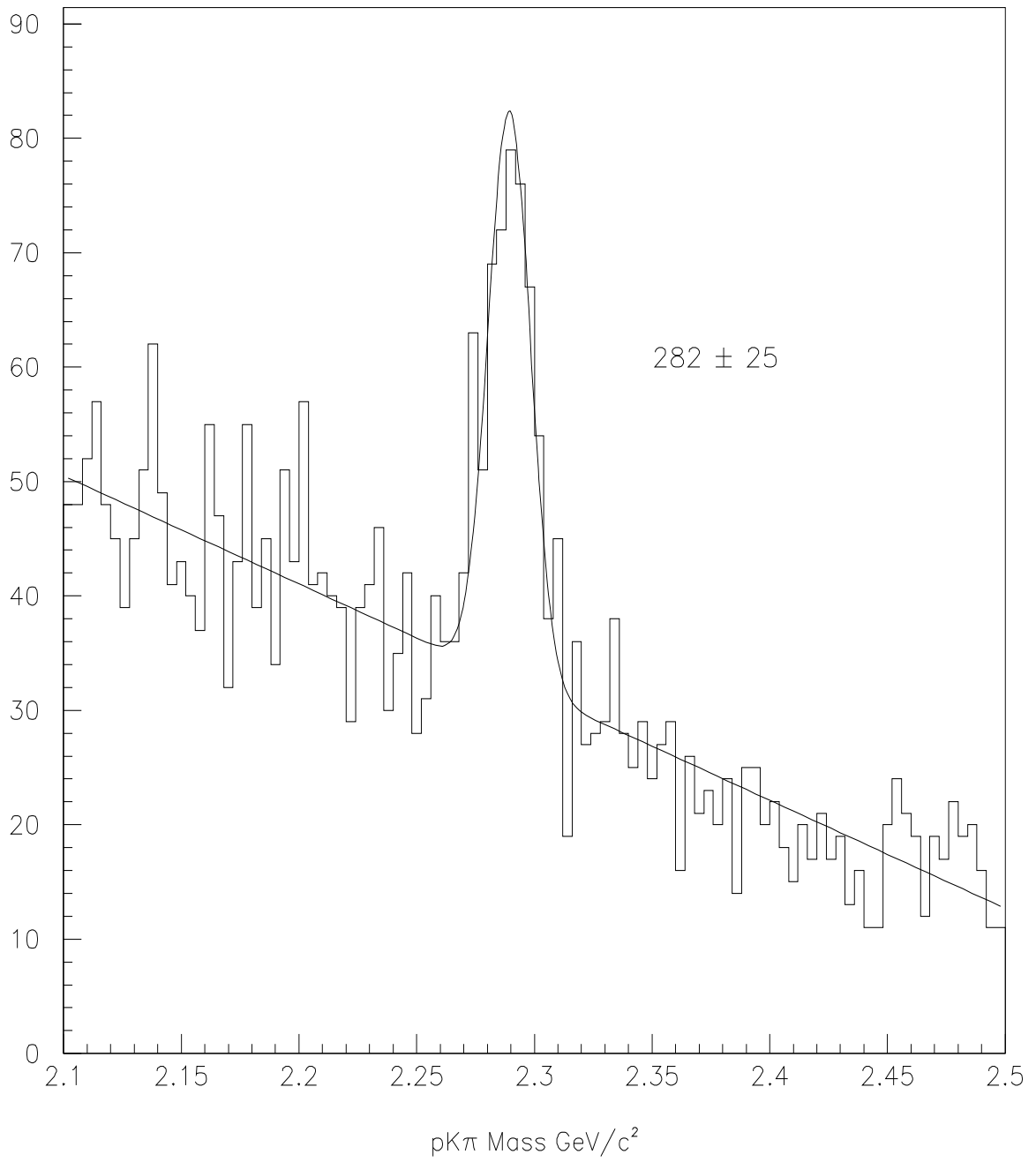


Figure 3.12:  $M_{pK\pi}$  with  $K^{*0}$  mass constraint.

We have made an estimate of the ratio of the efficiencies to be

$$\frac{\epsilon_{\Lambda_c \rightarrow p K^{\bar{*}0}}}{\epsilon_{\Lambda_c \rightarrow p K \pi}} = \frac{\rho_{\Lambda_c \rightarrow p K^{\bar{*}0}}^{Dalitz}}{\rho_{\Lambda_c \rightarrow p K \pi}^{Dalitz}} = 0.94 \pm 0.07 \quad (3.12)$$

Where  $\rho_{\Lambda_c p K \pi}^{Dalitz}$  is the number of all  $\Lambda_c \rightarrow p K \pi$  events per unit area in the Dalitz plot and  $\rho_{\Lambda_c p K^{\bar{*}0}}^{Dalitz}$  is the number of  $\Lambda_c \rightarrow p K^{\bar{*}0}$  events per unit area in the  $K^{\bar{*}0}$  mass window. If we assume that the  $\text{BR}(K^{\bar{*}0} \rightarrow K^- \pi^+) = 2/3$ , we calculate

$$\frac{BR(\Lambda_c \rightarrow p K^{\bar{*}0})}{BR(\Lambda_c \rightarrow p K \pi)} = 0.46 \pm 0.06 \quad . \quad (3.13)$$

We have ignored contributions from  $\Delta^{++} \rightarrow p \pi$  resonances and  $\Lambda^* \rightarrow p K$  resonances. We have also ignored the small corrections due to the tails of the Breit-Wigner shaped  $K^{\bar{*}0}(890)$  resonance. These effects are more easily handled by a full Dalitz plot analysis of  $\Lambda_c \rightarrow p K \pi$ .

# Chapter 4

## Conclusions

We have made a number of measurements relevant to charmed baryon physics. In this chapter I review the measurements and compare them to other previous measurements. Past charm particle measurements are nicely summarized in the article “Hadroproduction of Charm Particles” by J.A.Appel [17]. We will generally compare our results to the most recent high statistics measurements made by experiment NA32 at CERN and experiment E769 at Fermilab in  $\pi$ -N interactions. I will also comment on the improvements that can be made in the E791 measurements.

### 4.1 Measurements with $\Lambda_c \rightarrow pK\pi$

$\Lambda_c \rightarrow pK\pi$  has been our benchmark for checking charmed baryons decays. All of our measurements are based on this decay and with about 1000 reconstructed events, we have the world’s largest statistical sample at this time. We will make an estimate of the total inclusive cross section for producing  $\Lambda_c$ ’s in hadronic interactions and compare production results with others.

#### Estimate of the Total Cross Section

We can make an estimate of the total inclusive cross section,  $\sigma_{\Lambda_c}$ , following definitions and equation(1.5). The number of  $\Lambda_c$ ’s observed can be expressed as

$$N_{\Lambda_c}^{obs} = 2 \times L \cdot \sigma_{\Lambda_c} \cdot \bar{A}^{-1} \cdot BR(pK\pi) \cdot \epsilon_{pK\pi} \cdot \epsilon_{\Lambda_c}^{trig} \quad (4.1)$$

$L$  is the integrated luminosity.  $\bar{A}$  is the average atomic number of our target.

$$\bar{A} = \frac{\sum_i \rho_i \cdot \Delta t_i}{\sum_i \frac{\rho_i \cdot \Delta t_i}{A_i}} \simeq 20.5 \quad (4.2)$$

Where  $\rho_i$  is the density and  $\Delta t_i$  is the thickness of each target. The number of triggers can be expressed as

$$N_{trig} = L \times \sigma_{inelastic} \times \bar{A}^{2/3} \times \epsilon_{trig}^{inelastic} \quad (4.3)$$

Solving these two equations for  $\sigma_{\Lambda_c}$ , we get

$$\sigma_{\Lambda_c} = \frac{N_{\Lambda_c}^{obs}}{N_{trig}} \times \frac{\sigma_{inelastic}}{BR(pK\pi) \cdot \epsilon_{pK\pi}} \times \frac{1}{2} \times \frac{\epsilon_{trig}^{inelastic}}{\epsilon_{trig}^{\Lambda_c}} \times \frac{\bar{A}^{2/3}}{\bar{A}^1} \quad (4.4)$$

The factor of 1/2 accounts for the fact that there are on an average 2  $\Lambda_c$ 's per event. We have calculated  $A \simeq 20.5$  above for the effective target atomic number. If we assume that the trigger efficiencies are the same for inelastic and charm events then

$$\sigma_{\Lambda_c} = \frac{982 \pm 52}{13.3 \times 10^9} \times \frac{23mb}{(.044 \pm 0.006) \times (2.7 \times 10^{-3} \pm 6.4 \times 10^{-5})} \times \frac{1}{2} \times 0.37 \quad (4.5)$$

We arrive at  $N_{trig}$  by using an average of 815K evts/tape  $\times$  40 tapes  $\times$  364 runs =  $13.3 \times 10^9$ . We have assumed a branching ratio  $BR(\Lambda_c \rightarrow pK\pi) = 4.4 \pm 0.6$  % from the 1994 PDG [5]. We calculate a measurement of the total inclusive cross-section of

$$\sigma_{\Lambda_c} = (2.61 \pm 0.39) \mu b / N . \quad (4.6)$$

The error on the branching ratio dominates the statistical error on the cross-section measurement. We also give  $\sigma_{\Lambda_c} \cdot BR$  in the table (4.1) to show the full statistical power of our measurement.

This measurement is similar to the previous measurement as displayed in the table (4.1). Our largest uncertainties in this calculation are in the  $N_{trig}$  normalization and assumption about equality of trigger efficiencies. A more detailed study of cross-section vs target number will be needed to finalize this calculation. Although more work is needed to verify this calculation, we feel that these corrections are small.

	$\sigma_{\Lambda_c}(\mu\text{b}/\text{N})$	$\sigma_{\Lambda_c}.BR(\mu\text{b}/\text{N})$	$\frac{dN}{dX_F} = (1-X_F)^n$	$X_F \geq 0$
E791	$2.61 \pm 0.6$	$0.11 \pm 0.03$	$n = 5.8 \pm 0.65$	500GeV/c $\pi^-$ N
NA32	$4.1 \pm .5 \pm .7$	$0.18 \pm 0.02 \pm 0.03$	$n = 3.5 \pm 0.50$	250GeV/c $\pi^-$ N

Table 4.1: Comparison of production measurements with NA32

### $\Lambda_c^+/\Lambda_c^-$ ratio

We have measured the particle-antiparticle ratio in (3.3) to be

$$\frac{N_{\Lambda_c^+}}{N_{\Lambda_c^-}} = 1.14 \pm 0.12 \quad (E791) \quad . \quad (4.7)$$

It is consistent with being in the 1.0-1.2 range. NA32 has shown a similar result from a smaller number of hadro-produced events

$$\frac{N_{\Lambda_c^+}}{N_{\Lambda_c^-}} = 0.99 \pm 0.16 \quad (NA32) \quad (4.8)$$

E791's measurement covers a small range of negative  $X_F$  and should be more sensitive to the target diquark formulation of  $\Lambda_c^+$ . There is little evidence that this is a strong effect in the hadro-production for  $\Lambda_c$ 's. Our Lund hadronization Monte Carlo contains diquark formations. It would be instructive to investigate the charm particle ratios it provides.

### $X_F$ measurements

We have good acceptance for observing  $\Lambda_c$ 's produced near  $X_F = 0$ . Our momentum range for detecting  $\Lambda_c$ 's extends from  $X_F = -0.1$  to  $X_F = 0.4$ . We have fit our  $X_F$  spectrum to  $dN/dX_F \propto (1-X_F)^N$ . Our results for parameterization of the  $X_F$  distribution are given in table (4.1). With  $n \simeq 5.5$ , we see a very rapidly falling distribution. NA32 observes a more gradual decline in the  $X_F$  distribution which is more characteristic of the D meson production. E769 has measured for  $D^\pm$  production in 250 GeV/c  $\pi^-$ N interactions a power  $n = 3.21 \pm 0.24$  [17] .

## 4.2 $\Sigma_c$ measurements

We have observed evidence for  $\Sigma_c$  production with much difficulty, even with a very large and clean sample of  $\Lambda_c$  events. We see good evidence for  $\Sigma_c^0 \rightarrow \Lambda_c^+ \pi^-$  decays but little evidence for  $\Sigma_c^{++} \rightarrow \Lambda_c^+ \pi^+$ . Our  $\Sigma_c^0$  measurement indicates that the number of  $\Sigma_c^0$ 's produced relative to all  $\Lambda_c$ 's produced is about 13%. Its not understood why  $\Sigma_c^{++}$  is not easily observed. This is a significant observation and may have some impact on the fragmentation models. Isospin conservation predicts equal production of all  $\Sigma_c$ 's. In order to improve our signal to noise ratio in studying  $\Sigma_c \rightarrow \Lambda_c \pi$  decays, it is essential that we have better selection of pions associated with  $\Sigma_c$  decays in the primary vertex. Further studies on selecting this pion must be done. Our final calculation of the ratio  $N_{\Sigma_c}$  to  $N_{\Lambda_c}$  gives

	$\Sigma_c^0$	$\Sigma_c^{++}$
$\frac{N_{\Sigma_c}}{N_{\Lambda_c}}$	$0.09 \pm 0.022$	$0.04 \pm 0.016$

Table 4.2:  $\Sigma_c$  production measurements.

## 4.3 $\Lambda_c \rightarrow pK^{\bar{*}0}$ measurement

Our measurement of  $\Lambda_c \rightarrow pK^{\bar{*}0}$  clearly indicates that this decay channel dominates  $\Lambda_c \rightarrow pK\pi$  decays. The latest Particle Data Group measurement [5] gives

$$\frac{BR(\Lambda_c \rightarrow pK^{\bar{*}0})}{BR(\Lambda_c \rightarrow pK\pi)} = 0.36 \pm 0.1 \quad (PDG) \quad (4.9)$$

The E791 measurement is

$$\frac{BR(\Lambda_c \rightarrow pK^{\bar{*}0})}{BR(\Lambda_c \rightarrow pK\pi)} = 0.46 \pm 0.06 \quad (E791) \quad (4.10)$$

The E791 measurement gives an enormous increase in the statistical certainty. A proper treatment of this measurement can only be made through a full Dalitz plot analysis.

## 4.4 Summary

We have observed a large and clean sample of  $\Lambda_c \rightarrow pK\pi$  decays in E791. We were able to present measurements on production and decay with high statistical accuracy. It is doubtful that our  $\Sigma_c$  measurements in E791 will be of high quality due to unavoidable backgrounds from our high multiplicity events. As indicated, further studies are needed on all of the analyses.

### Systematic Errors

In this thesis we have made no attempt to assign systematic errors to our calculations. This will be essential for the publication of the data. In each section we have stated assumptions that are made and suggested further studies.

# Bibliography

- [1] S.Weinberg, *Phys. Rev. Lett* **19**, 1264 (1967).  
A.Salam, *Elementary Particle Theory*, N.Svartholm, ed. (Stockholm: Almquist and Wiksell, 1968).
- [2] B.J. Bjorken and S.L. Glashow, *Phys. Rev. Lett.* **11**, 255 (1964).
- [3] S.L. Glashow, J. Iliopoulos and L.Maiani. *Phys. Rev. Lett.* **D2**, 1285 (1970)
- [4] J.J. Aubert et al., *Phys. Rev. Lett.* **33**, 1404 (1974).  
J.E. Augustin et al., *Phys. Rev. Lett.* **33**, 1406 (1974).
- [5] Particle Data Group, *Phys. Rev.* **D50**, 1173 (1994).
- [6] B.L.Combridge, *Nuclear Physics* **B151**, 429-456 (1979).  
David Griffiths, “Introduction to Elementary Particle Physics”, 1987 John Wiley & Sons, Inc.
- [7] P. Nason, S. Dawson, and R.K. Ellis, *Nucl. Phys.* **B327**, 49 (1989).
- [8] S. Barlag, et al., *Phys. Rev. Lett* **B247**, 113 (1990).  
J.C. Anjos, et al., *Phys. Rev. Lett* **62**, 15 (1989).
- [9] Bowcock et al., *Phys. Rev. Lett* **62**, 1240 (1989).
- [10] L. M. Cremaldi, “E691 Dalitz Plot Analysis of  $\Lambda_c^+ \rightarrow pK\pi$  Decays”, presented at the *E791 Physics Workshop* 1992, Santa Cruz CA.

- [11] S.Amato et al., Nucl. Inst. Meth. **A324**, 535 (1993).  
 D.Bartlett et al., Nucl. Inst. Meth. **A260**, 55 (1987).  
 J.A. Appel et al., Nucl. Inst. Meth. **A243**, 361 (1986).  
 V.K.Bharadwaj et al., Nucl. Inst. Meth. **228**, 283 (1985).  
 D.J.Summers,Nucl. Inst. Meth.**228**, 290 (1985).  
 V.K.Bharadwaj et al., Nucl. Inst. Meth **155**, 411 (1978).
- [12] D.J. Summers et al., “Charm Physics at Fermilab E791” Proceedings of the XXVII<sup>th</sup> Rencontre de Moriond, Electroweak Interactions and Unified Theories, Les Arcs, France 417 (1992).
- [13] M .V. Purohit, “Momentum and mass resolutions on E791”, E791 Online Document 161.
- [14] S. B. Bracker et al., “A Simple Multiprocessor Management System for Event-Parallel Computing” **BaBar Note 128**, Stanford Linear Accelerator.
- [15] T. Carter, E791 at Fermilab, Private communication.
- [16] L. M. Cremaldi, E791 at Fermilab, Private communication.
- [17] J.A. Appel, “Hadroproduction of Charm Particles”,*Annu. Rev. Nucl. Part. Sci* **42**, 367-399 1992.